IEEE Access
Multidisciplinary | Rapid Review | Open Access Journal

Received 16 November 2022, accepted 12 December 2022, date of publication 23 December 2022,
date of current version 29 December 2022.

Digital Object Identifier 10.1109/ACCESS.2022.3231984

TOPICAL REVIEW

Review on Substrate Integrated Waveguide Cavity Backed Slot Antennas

ELAGANDULA APARNA, (Graduate Student Member, IEEE), GOPI RAM, (Senior Member, IEEE), AND G. ARUN KUMAR, (Senior Member, IEEE)
Department of Electronics and Communication Engineering, National Institute of Technology Warangal, Hanamkonda 506004, India
Corresponding author: Gopi Ram (gopi.ram@nitw.ac.in)

ABSTRACT Substrate Integrated Waveguide Cavity Backed Slot Antennas (SIW CBSA) are emerging candidates for planar Integrated Circuit (IC) technology in Millimetre-wave (MMW) bands. This peculiar antenna holds the advantage of conventional metallic cavity-backed antennas, with high gain, high front-to-back ratio, and low cross-polarization level. SIW CBSA structures are the best option for planar integration with a low profile and low fabrication cost in the design of MMW systems. This paper discusses various forms of SIW CBSA structures, their operating mechanism, and methods of improving their performance in terms of gain, bandwidth, size reduction, beamforming capability, and multiple bands of operation. From this discussion, we can select the antenna with the required characteristics of gain, dual-band, and dual-polarization suited for present and future-generation applications.

INDEX TERMS Beam steering antennas, circular polarization, dual-band, dual-polarized, double slot antennas, fifth-generation, large-frequency ratio, MMW band, reconfigurable antennas, SIW CBSA.

I. INTRODUCTION

Wireless components and systems have been in demand with increased interest for present 5G wireless communication systems. The 5G spectrum consists of a sub-6 GHz band and Millimeter-wave (MMW) band (24 -100 GHz). The MMW band utilization benefits the end-users with high bandwidth and data rate and decreases the data traffic. With the advantages of MMW bands, they are highly utilized in wireless communication systems. In the MMW band, 60 GHz unlicensed band utilization for wireless networks [1], imaging sensors [2], automatic radars, security devices [3], and more applications have been proposed. The usage of the MMW band supports the evolution of wireless systems with a high amount of speed, data rate, capacity, resolution, and broadband systems. It is experimentally proved that 28 GHz and 38 GHz bands are highly suitable for Fifth-generation communication systems [4]. MMW band frequency high-level applications are mentioned in Fig. 1 [5]. For any wireless system, oscillators, mixers, and low-noise amplifiers have been considered core active elements. These functional elements are embedded in a chipset at a low cost, but antennas, filters, and power amplifiers can't be easily embedded with active components at MMW frequencies. So, the development of a planar platform with reliable technology for such circuits is advantageous in mm-wave wireless systems.

Substrate Integrated Waveguide technology (SIW) is a good choice for designing such a planar platform. For two decades, SIW technology has gained more attention in high-frequency bands to design microwave and MMW planar circuits due to their planar integration capability. The first planar waveguide line was proposed by Shigeki, F. in 1994 [6]. The dielectric substrate is embedded with arraying metal vias on two side walls to build waveguides in planar form is called a post-wall waveguide (laminated waveguide) structure, as shown in Fig.2. These waveguide characteristics are analyzed using a post-wall waveguide structure [7]. The leakage of electromagnetic waves in post-wall waveguides is suppressed in a laminated waveguide structure. Such laminated waveguide structures are restored with the inherent merits over conventional nonplanar waveguide structures, called Substrate Integrated Waveguide structures [8]. The SIW structures enable the planar integration of the three-dimensional structures at MMW

The associate editor coordinating the review of this manuscript and approving it for publication was Guido Valerio.

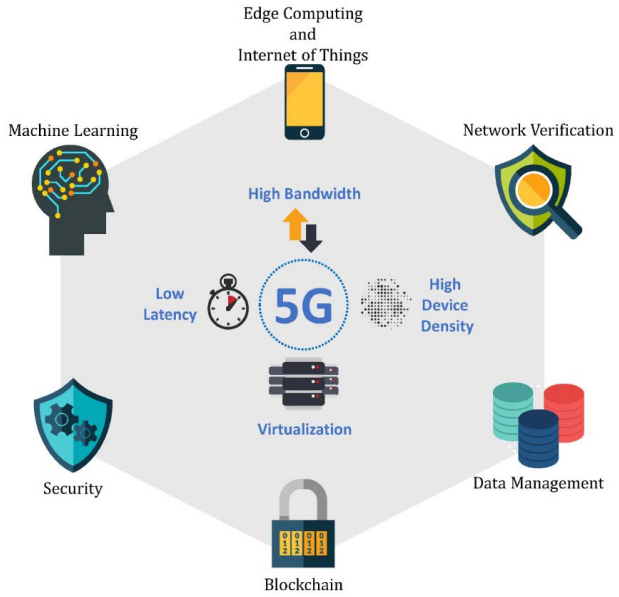

FIGURE 1. Millimetre-wave (MMW) frequency usage scenarios [5].

frequencies. These SIW devices are manufactured either with the Printed Circuit Board (PCB) technology or Low-temperature co-fired ceramic (LTCC) technology [6]. They are low-cost, lightweight, and simple to build compared to conventional metallic waveguides [9]. These SIW devices have challenges like dielectric losses and low power handling capability compared to a conventional waveguide. The dielectric substrate embedded in SIW increases the dielectric losses. Deslandes et al. proposed that by increasing the substrate thickness, conductor loss and dielectric losses are minimized, and the corresponding attenuation constant is inversely proportional to substrate thickness. The other geometrical dimensions of SIW have a negligible effect on conductor losses. Depending upon operating frequency, the substrate thickness is chosen to make the attenuation constant a low value. For example, at terahertz frequency, substrate size is limited to 0.254 mm, and at the MMW band, the substrate thickness is chosen maximum up to 0.787 mm [10]. Different types of SIW cavity-backed slot antenna construction details and operating principles proposed at the MMW band and microwave bands were the subject of this review.

This review manuscript is categorized as follows, and section II discusses the fundamental theory and construction details of SIW structures. Section III contains a technical review of several published papers on SIW cavity-backed slot antennas and arrays, large frequency ratio integrated antennas, SIW dual-slot antennas, and reconfigurable antennas. Section IV summarizes and concludes with future scope.

II. DESIGN RULES FOR SIW STRUCTURES

The SIW structure is orchestrated by two rows of vias implanted in a dielectric substrate with top and broad bottom walls that works as conducting plates, as shown in

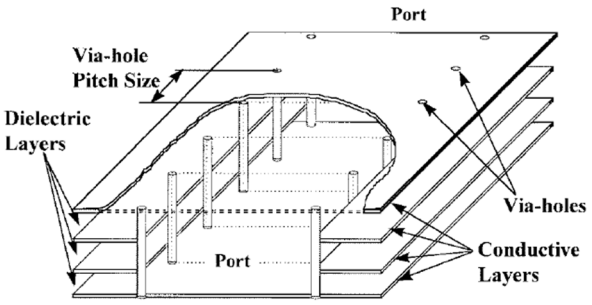

FIGURE 2. Schematic diagram of post-wall waveguide structure [6].

Fig. 3 (a) and (b). Two rows of vias act as narrow walls of the SIW structure. Most of the advantages of the conventional Rectangular Wave Guide (RWG) structure are preserved in the SIW structures, and full-scale integration is an attractive feature of SIW structures at MMW bands [9]. Design Rules of the SIW structures are discussed in [9] and [10]. Boundary Integral Resonant Mode Expansion (BI-RME) method and the Floquet theorem are combined to investigate the dispersion properties of the SIW structures and conclude that the SIW exhibits similar dispersion characteristics as the conventional RWG by assuming that the effective width of SIW is equal to the conventional RWG.

The effective width of SIW can be derived from Eq. (1) as follows [11]

$$w_{eff} = w - \frac{d^2}{0.95 * s} \tag{1}$$

where d is the via diameter, w is the width of the SIW structure, and s is the adjacent pitch distance between metal vias. Referring to (1), it does not consider the effect of d/w, so modified empirical Eq. (2) is defined by the multimode numerical calibration procedure in [12].

$$w_{eff} = w - \frac{1.08 * d^2}{s} + 0.1 * \frac{d^2}{w} \tag{2}$$

The propagation characteristics of SIW were analyzed by the Method of Lines (MoL) as provided in Eq. (3) [13].

$$w = \left(\xi_1 + \frac{\xi_2}{\frac{s}{d} + \frac{\xi_1+\xi_2-\xi_3}{\xi_3-\xi_1}}\right) \text{for } \mathrm{TM_{x0n}} \text{modes} \tag{3}$$

where ξ_1, ξ_2, and ξ_3 are constants, and the following equations express those values.

$$\xi_1 = 1.0198 + \frac{0.3465}{\frac{w}{s} - 1.0684}$$

$$\xi_2 = -0.1183 - \frac{1.2729}{\frac{w}{s} - 1.2010}$$

$$\xi_3 = 1.0082 - \frac{0.9163}{\frac{w}{s} + 0.2152}$$

To prevent radiation leakage from the adjacent vias in the SIW structure, it should satisfy the following conditions in Eq. (4)

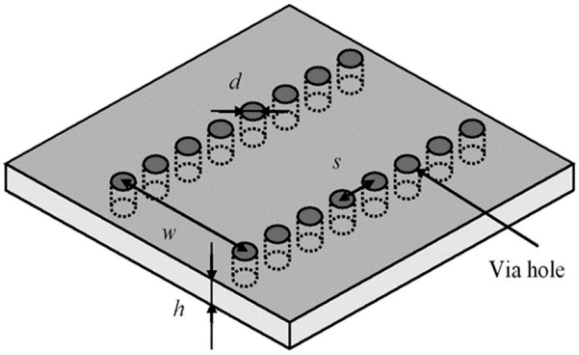

(a)

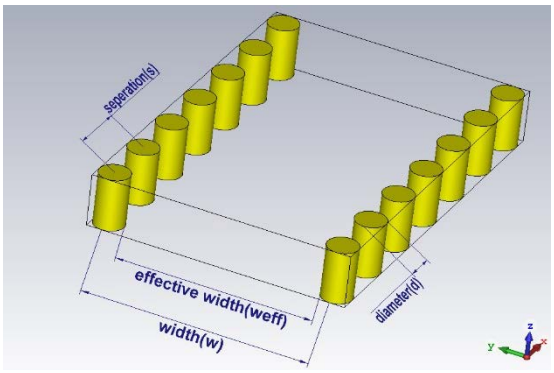

(b)

FIGURE 3. (a) Configuration of SIW structure [8]. (b)Two rows of vias with the parameter labelled in CST.

for the SIW cavity [12].

$$d < \frac{\lambda_g}{5}, s \leq 2d \tag{4}$$

where, λ_g is the guided wavelength of propagating wave in SIW [14].

$$\lambda_g = \frac{\lambda_0}{\sqrt{\varepsilon_r - \left(\frac{\lambda_0}{\lambda_c}\right)^2}} \tag{5}$$

where, λ_o operating wavelength and λ_c The cutoff wavelength of the wave.

III. TECHNICAL REVIEW

A. SIW CAVITY BACKED SLOT ANTENNA

J.Hirokawa et al. proposed a Conventional Cavity Backed Slot Antenna (CBSA) with wide bandwidth in 1989 [15]. Afterwards, its features, such as high gain, high front-to-back ratio, and unidirectional pattern, make the conventional CBSA a good choice for wireless communication systems. From Fig. 4, we can observe tha conventional CBSA is bulky and has a nonplanar structure. Integrating these nonplanar structures is complex and requires extra hardware components. The integrity problems were eliminated by designing a CBSA with SIW technology which facilitates a planar, low-cost waveguide structure. Some of the SIW CBSA with

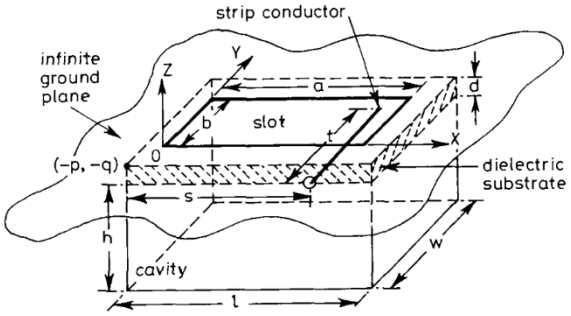

FIGURE 4. Conventional Cavity Backed Slot Antenna [14].

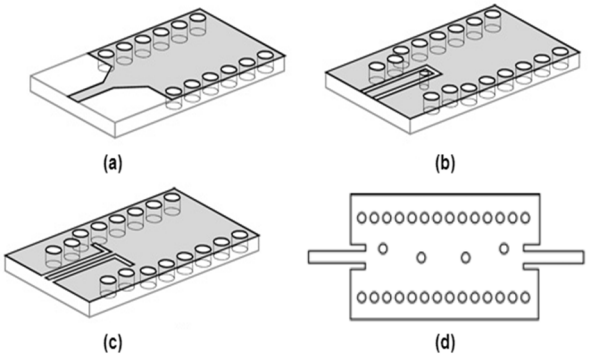

FIGURE 5. Transition between SIW and transmission lines (a) Microstrip to SIW transition structure. (b) Coplanar to SIW transition with the current probe. (c) Coplanar to SIW transition with 90° Bend. (d) SIW Filter with an inductive post.

integration has been presented for integrability purposes in [9] and [10]. A new construction method is used to design the waveguide with the help of SIW structures, as shown in Fig. 5(a). Here microstrip line and rectangular waveguide are connected via a simple tapering module on the same substrate. This new transition helps design a complex waveguide component in planar form.

As shown in Fig. 5 (b) & (c), a coplanar waveguide and a rectangular waveguide are fully integrated on the same substrate to make planar circuits without any additional mechanical tuning to operate at the MMW band as proposed in [16]. Power dividers are also designed in a planar form using the standard PCB process. These planar SIW power dividers have been basic building blocks for designing complex microwave circuits. For the First time, Li-yan et al. experimented with SIW slot array antennas by loading the longitudinal slots on the top conducting layer of SIW [17]. The proposed design is advantageous compared to conventional waveguide slot array antennas in terms of size, weight, and cost, with a slight decrement in gain and efficiency.

Primarily, the slot and cavity dimensions have been calculated for the same resonant frequency with the excitation of TE_{101} mode. The cavity dimensions are calculated in Eq. (6) [13].

$$f_r(TE_{101}) = \frac{1}{2\sqrt{\varepsilon\mu}}\sqrt{\left(\frac{1}{w_{eff}}\right)^2 + \left(\frac{1}{L_{eff}}\right)^2} \tag{6}$$

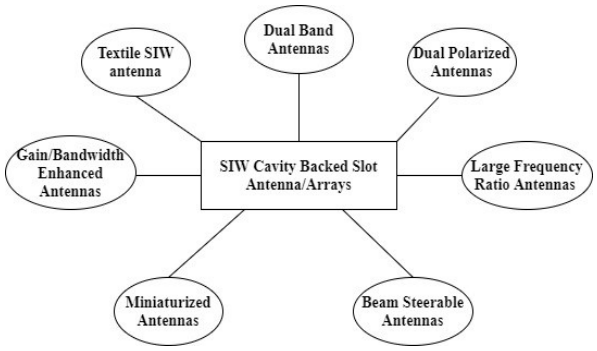

FIGURE 6. Classification of SIW CBSA Antenna/Array.

where ε is permittivity, μ is permeability, W_{eff} and L_{eff} are effective width and length of the SIW cavity, respectively. The SIW cavity width and length (W_{siw} and L_{siw}) can be approximated as follows in Eq. (7) & Eq. (8) [11]:

$$W_{siw} = W_{eff} + \frac{d^2}{0.95 * s} \tag{7}$$

$$L_{siw} = L_{eff} + \frac{d^2}{0.95 * s} \tag{8}$$

where d and s parameters are similar to the parameters discussed in SIW design. To minimize the guided power leakage from the sidewalls of the cavity, the geometry of the linear array of vias should follow Eq. (4) and (5), which are discussed in the earlier section. Based on the utilization of SIW structures, several types of antennas are implemented for high-frequency applications. SIW CBSA array classification is listed in Fig. 6.

Some of the proposed research is discussed in detail to understand SIW CBSA configurations. Miniaturized SIW slot antennas based on negative order resonance are proposed in [18] and [19]. SIW CBSA's are loaded with metamaterials to achieve a good amount of miniaturization. As shown in Fig.7(a), an interdigital slot is loaded on the top plane of the SIW cavity to operate the resonator as Composite Right Left-Handed (CRLH) SIW resonator [18]. A ramp-shaped slot is loaded on the SIW cavity to perform the resonator presented in Fig.7(b) in the first negative order mode resonance [19]. The proposed antenna in [19] achieves 87% miniaturization with a gain of 3.6 dBi at 2.1 GHz. From [18] and [19], we can conclude that even the antenna resonates in lower frequencies instead of increasing the size, slots are loaded with capacitive loading to operate in the negative order mode with the same size. Due to the loading effect, antenna size remains unchanged, and miniaturization is achieved.

Earlier, a fragile cavity-backed microstrip-fed slot antenna is investigated in [20]. This work provides a path to design cavity-backed slot antennas in SIW structures. A thin cavity-backed crossed slots antenna is proposed to operate at 2.34 GHz for dual broadcast systems such as satellite radio and terrestrial communication [21]. A novel design method of low-profile SIW CBSA is described in [22]. A grounded

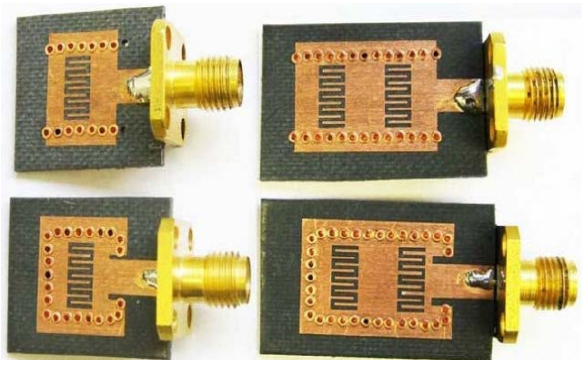

(a)

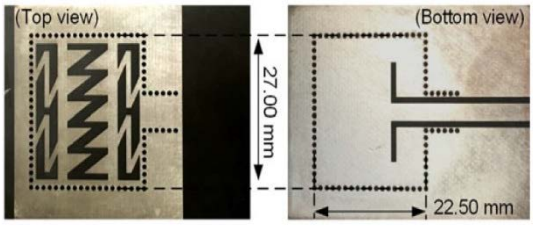

(b)

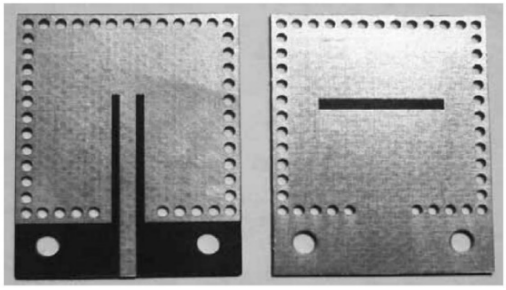

(c)

FIGURE 7. (a) SIW antenna with IDC structures [18], (b) An ultra-Miniature SIW CBSA [19], (c) a very thin cavity SIW CBSA structure [22].

TABLE 1. CBSA topology and characteristics.

Ref	Topology	f_r (GHz)	Gain(dBi/dBic)
[18]	SIW CBSA with metamaterial	2.10	3.6
[21]	Waveguide with crossed slots	2.34	1.1(VP),1.2(HP),2.2(LHCP),9.1(RHCP)
22]	SIW CBSA with GCPW	10	5.4

f_r: operating frequency

coplanar waveguide (GCPW) feed line excites the TE_{120} mode in the cavity resonator.

The slot length is chosen in such a way that the E- field across the sides of the slot has a phase reversal, and energy can radiate into space. Here $19.8 \times 23.8 \times 0.5 mm^3$ size, CBSA is presented as shown in Fig. 7(c). It has achieved a gain

of 5.4 dBi, Front to Back Ratio (FTBR) of 16.1 dB, and 1.7% bandwidth at 10 GHz frequency. From this article [22], we can observe that the impedance bandwidth is affected by substrate thickness and slot width. A half-wavelength dimension slot is considered for better radiation efficiency at the resonant frequency. The radiation patterns of the crossed slot antenna vary from Left Hand Circular Polarization (LHCP) in the elevational direction to Vertical Polarization (VP) at the horizon. Here crossed-slot aperture utilizes the dual resonance technique for circular polarization. By utilizing the crossed slots, in the far-field region, radiation from the two orthogonal slots with 90^0 phase differences produces Circular Polarization (CP) towards the elevational direction. The slots and cavity are tuned together to get the radiating modes. The cavity thickness and slot width dimensions are optimized to improve the operational bandwidth. Here crossed slots loaded cavity antenna supports four modes. The two modes are related to crossed slots, and two additional modes are related to interference. SIW CBSA with different slot configuration characteristics is compared in Table 1. We discussed low-profile CBSA and miniaturized antennas earlier. Apart from that, bandwidth enhancement of low-profile CBSA is proposed in [23]. In the proposed design combination of TE_{110} and TE_{120} modes is excited in the SIW-backed cavity, as shown in Fig. 8. Wide bandwidth is achieved by utilizing the two-hybrid modes. Impedance bandwidth is enhanced from 1.4% to 6.3%, and its gain is slightly improved. There are several techniques, like increasing the substrate thickness and utilizing dual modes in the SIW cavity to improve the bandwidth, But these antennas usually suffer from a lower value of gain. The cavity-backed patch antenna grabbed particular interest to enhance the bandwidth [24], [25].

A wideband SIW cavity-backed E-shaped Patch Antenna is shown in Fig. 9(a) [24]. This structure consists of three metallization layers and two substrates. The top metal layer is loaded with E-shaped patches, a feedline line with vias and tunable loads working as a feeding structure in the middle layer, and the bottom layer behaves as a ground plane. Here E shaped patches are excited with feeding vias connected to the strip line, as shown in Fig. 9 (a). From Fig. 9 (b), we can observe that a lower resonant frequency (f_L) can't be created with E shaped patch antenna because the probe inductance is very low and the patch and ground exhibit a large capacitance value.

To enhance the inductance value at a lower resonant frequency, tunable stubs are connected across feeding via in middle layer. By properly selecting the length and width of stub parameters lower resonant mode is excited. Without loaded stubs, E shaped patch antenna resonates at f_R and which is slightly lower than the higher resonant frequency (f_H). After loading the stub parameters f_L and f_H are created. The proposed E-shaped patch single elements design achieves a bandwidth of 10.9%, and a gain of 7.7 dBi, while a 2×2 array achieves a bandwidth of 10.5%, and a gain of 13.2 dBi for X band applications. For modern wireless communication, dual-.polarized, high gain, and broadband

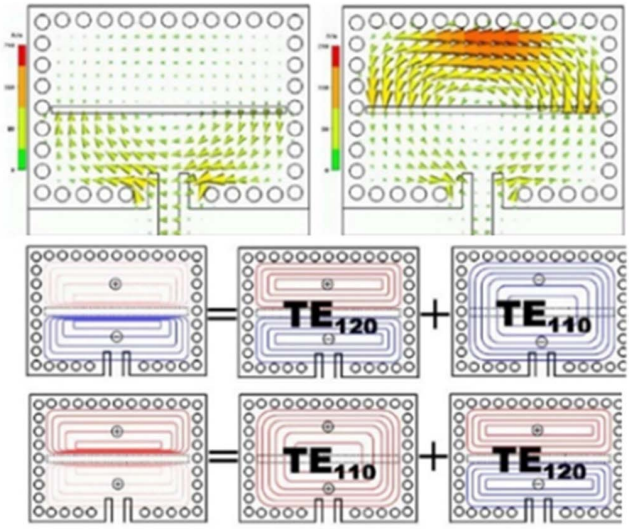

FIGURE 8. Hybrid modes representation in SIW CBSA [23].

antennas are desirable to improve the link quality, and communication capacity [5]. Different types of SIW-fed array configurations are presented in [26], [27], [28], and [29] to improve bandwidth and gain. However,

Substrate loss is dominant at the MMW band when designing a broadband, dual-polarised high-gain antenna. In [26], a SIW fed patch antenna array in a multilayer structure with high gain and bandwidth for the 60 GHz band. The proposed antenna is suitable for future mm-wave wireless communication. A 4×4 antenna array is designed to achieve a 27.5% and 22.6% bandwidth and 19.6 dBi gain. In [27], they have adopted a dual-polarized Magneto Electric (ME) dipole array with air-filled cavities and metallic pillars to minimize substrate loss. By adopting the ME dipoles in the SIW feed array, broadband and high gain in a unidirectional pattern with a lower cross-polarisation value are achieved.

The proposed 8 × 8 dual-polarized antenna array 3-D view is shown in Fig.10 (a). It consists of four layers, ME dipole array in the top layer, 1 to 4 power divider in the second layer, port 1 in the third layer, and port 2 in the fourth layer. Measurement and simulated results are compared in Fig.10 (b). Semicircle cut edges are introduced on the conventional cross-shaped slots to improve the bandwidth of the antenna array [28]. In this article, a dual-layer SIW feed CBSA array (8 × 8) is constructed to obtain a gain of 22.3 dB for 60 GHz applications.

An aperture-coupled vertical network couples the power to the second metal layer. A slot is etched on the bottom metal layer for H-polarization (H-pol). A cross-shaped slot is inscribed simultaneously on the middle layer for Vertical/Horizontal-Polarized. Semicircle cut on the slot edges introduces new resonances in the higher band. By increasing the diameter of the semicircles, these multiple resonances at high frequencies are merged, and board bandwidth is achieved. The fabricated prototype of the

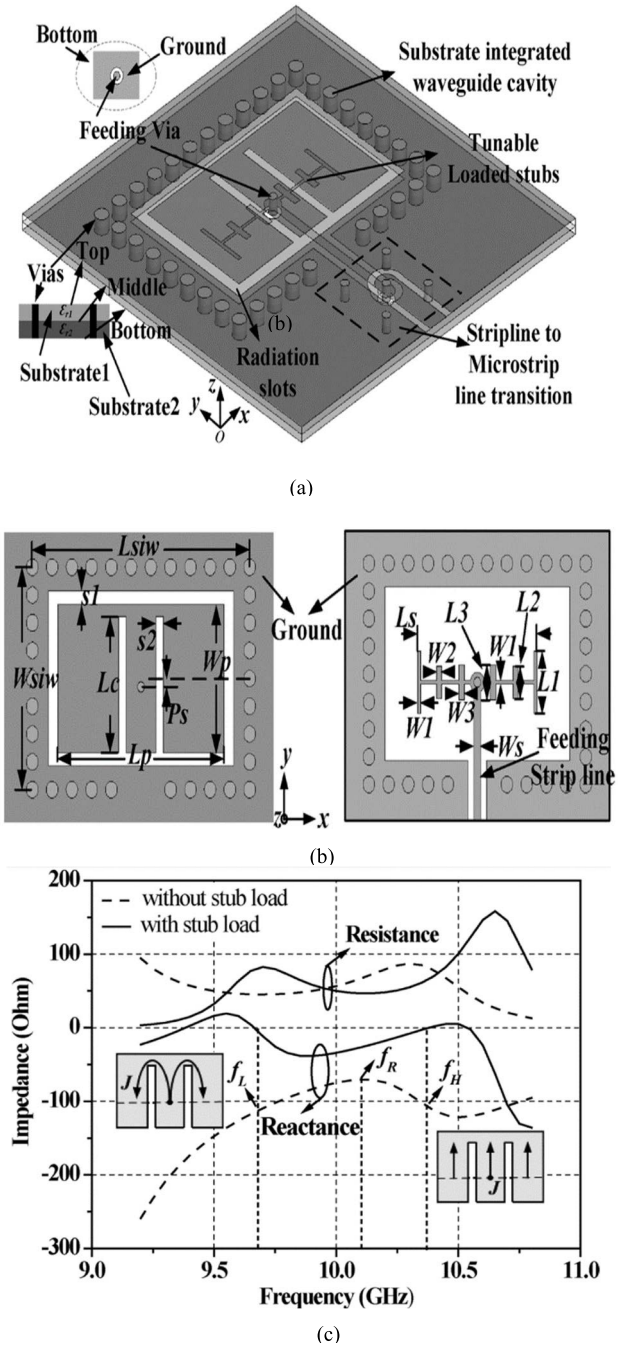

FIGURE 9. Bandwidth-enhanced low-profile SIW CBSA structure [24] (a) E Shaped Patch antenna in SIW cavity structure. (b) enlarged view of the E patch antenna with stubs in a ground plane (c) The impedance characteristics of the proposed antenna. $W_{siw} = 18.6, L_{siw} = 13.2, L_c = 10, L_p = 14.2. W_p = 9, P_s = 0.5, s_1 = 0.8, s_2 = 0.6, L_1 = 3.7, W_1 = 0.2, L_2 = 1.9, W_2 = 0.4, L_3 = 2.1, W_3 = 0.4, L_s = 10, W_s = 0.6.$

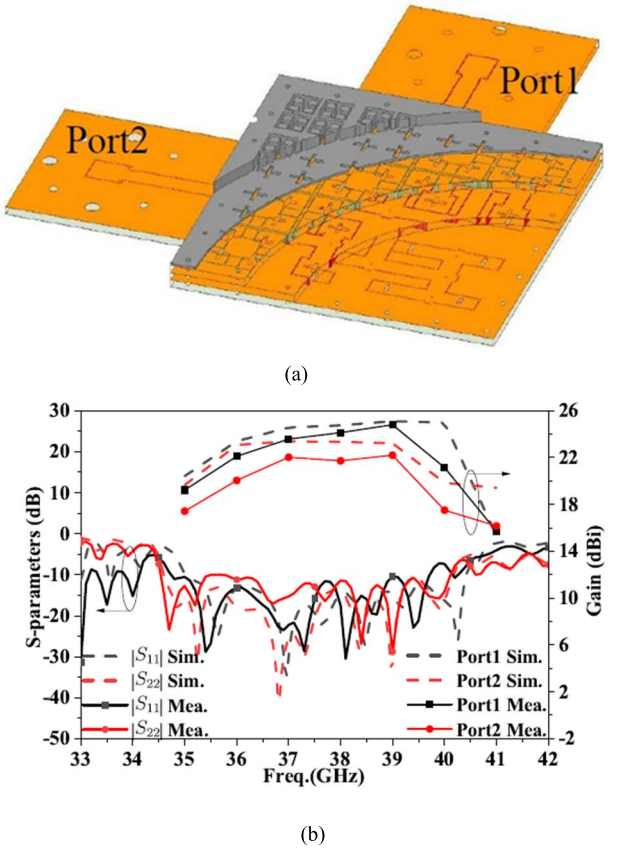

FIGURE 10. SIW fed Magneto Electric (ME) dipole (a) fabricated 8 × 8 ME dipole antenna array (b) S parameters and gain of 8 × 8 antenna array (Measured and Simulated) [27].

TABLE 2. Comparison table of SIW CBSA arrays at 60 GHz applications.

Ref	Array Elements	Gain (dBi)	IBW(%)	η (%)	Pol
[26]	4×4	19.6	27.5	54.5	LP
[27]	8×8	24.8	14.4	NA	HP, VP
[28]	8×8	22.3	17.1	70	HP, VP
[29]	8×8	26.7	22.9	80	LP

IBW: Impedance Bandwidth, η -efficiency, Pol-Polarization

8 × 8 semicircular antenna array is presented in Fig.11(a), and the return loss characteristics of H-pol and V-pol antennas are presented in Fig. 11(b). An array of antenna elements 2 × 2, 4×4, and 8 × 8 configurations are analyzed in [29] for covering the 50-74 GHz band applications. The proposed antenna element consists of slots surrounded by two dipoles in parallel for better performance. The measurement values of fabricated antenna prototypes discussed in [26], [27], [28], and [29] are presented in Table 2.

Discussion: We have discussed low-profile SIW CBSA, and miniaturized antennas. This low-profile antenna BW and gain are improved by increasing the substrate layers by utilizing the dual resonant modes in the cavity. These planar antennas with high integration capability can be used practically. But practically high gain dual polarized dual-band with a large frequency ratio or small frequency ratio is required. In the future for 5G and beyond applications System In Package (SIP) chipsets are required.

B. DUAL-BAND ANTENNAS

If we look into satellite communication applications, an antenna operating at a dual-band with a small frequency ratio is required. In [30], based on the advantage of aperture

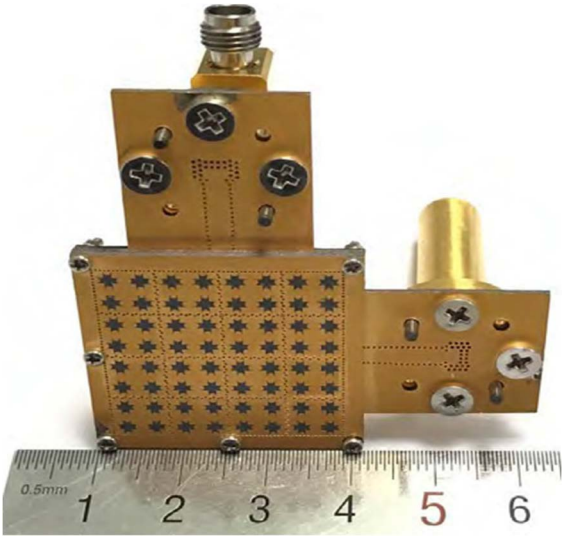

(a)

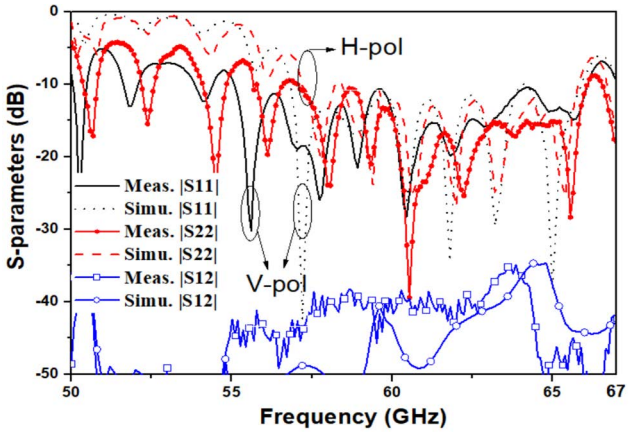

(b)

FIGURE 11. (a) An 8×8 dual-polarized semicircular cross-shaped slot antenna array, (b) S parameters of the proposed antenna array [28].

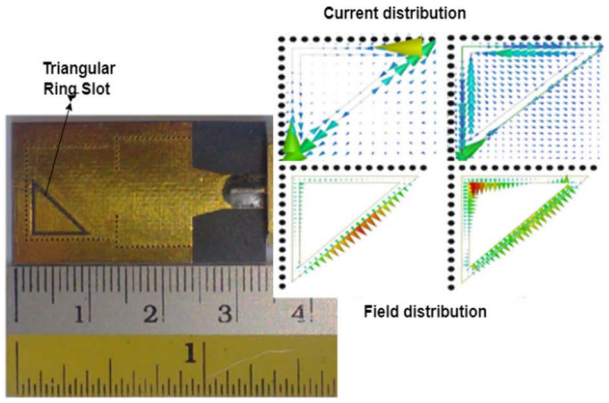

(a)

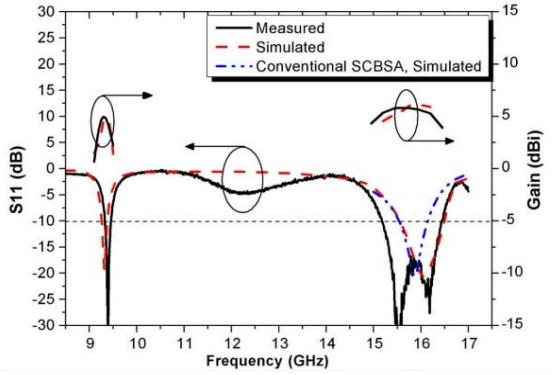

(b)

FIGURE 12. (a) Photograph of fabricated dual-band SIW cavity-backed TRS antenna with surface current and E- field distributions in the TRS slot at two frequencies. (b) Return loss characteristics [31].

sharing a dual-band shared aperture antenna array for MMW bands(K-/Ka-bands) is proposed for low earth orbit (LEO) satellite communication. In another method, SIW CBSA is reported as operating in the dual-band by exciting two different modes in design [31], [32], [33], [34]. A dual-band operating frequency is obtained by simultaneously exciting the two modes in the triangular ring slot (TRS) [31]. This resonant operation can be analyzed with the help of field distributions in the TRS as shown in Fig.12(a). At lower frequencies TRS radiates and at higher frequencies patch inside the TRS is radiated. The fabricated SIW cavity-backed TRS antenna is presented in Fig.12(a) and return loss characteristics are presented in Fig.12(b).

In [32], a novel dumbbell-shaped slot is introduced to create additional hybrid modes without disturbing the conventional TE_{120} mode. The frequency ratio of two bands can be tuned to certain values by changing the dimension of the slot. Design details and return loss characteristics are presented in Fig.13.

In [33], A Dual-band Cavity-backed SIW array antenna with a small size is presented. This dual-band is achieved by exciting higher-order hybrid mode (TM_{310}+TM_{130}) and second higher-order mode (TM_{320}) into the SIW cavity by an inductive window. The proposed 2 × 2 elements design, as shown in Fig.14 (a) and (b), achieves a gain of 16 and 17.4 dBi, respectively, at two operating bands (21 and 26 GHz).

In [34], A Dual-band circularly polarized SIW cavity-backed slot antenna is presented. Two annular exponential slots are carved on the surface of the SIW cavity to excite the cavity mode and surface mode. A two-order matching circuit using an inductive window is presented with the help of the differential evolution method to achieve dual-band operation. The proposed antenna operates at 37 and 48 GHz bands, as shown in Fig.15.

This dual-band SIW CBSA is rarely involved due to the improper frequency ratio of bands [31], [34]. Proximity-coupled slot apertures are used to excite the two consecutive

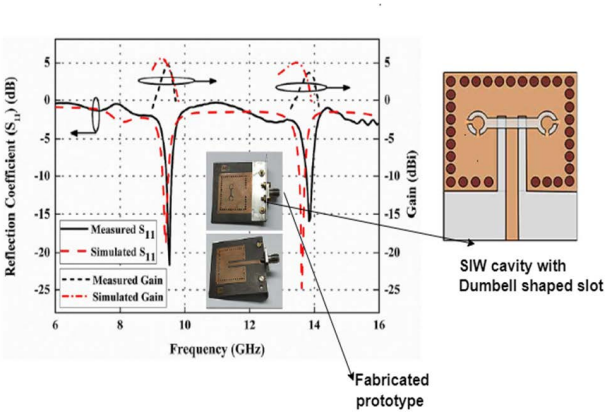

FIGURE 13. (a) Return loss characteristics of SIW cavity-backed dumbbell-shaped slot antenna [32].

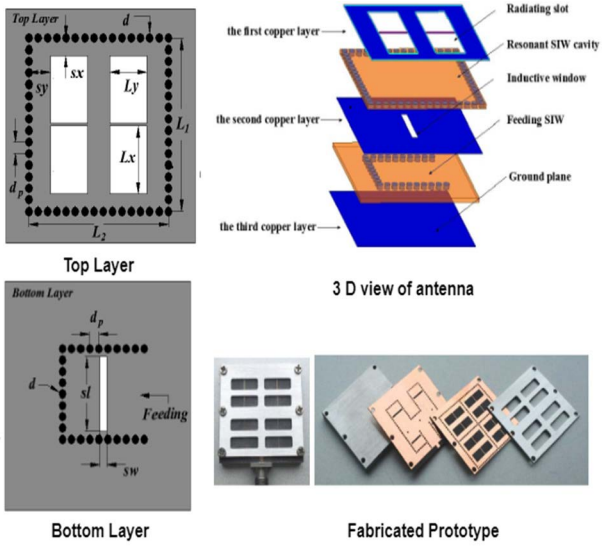

(a)

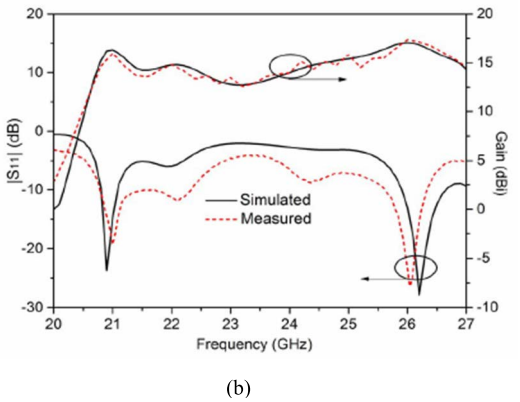

(b)

FIGURE 14. (a) Four-layer antenna with the fabricated prototype (b) Return loss characteristics of the proposed antenna in [33].

resonant modes (TM_{020} and TM_{120}). Meanwhile, degenerate polarization modes are depressed [35]. In [35], a SIW circular cavity is constructed with two rectangular slots as radiators on the top plane, and a rectangular SIW with a power divider

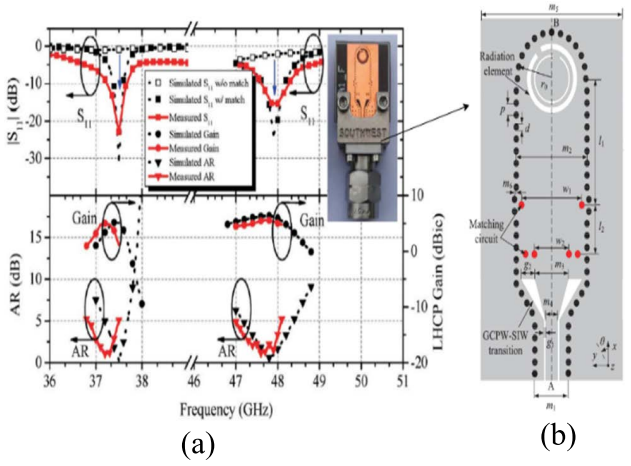

(a) (b)

FIGURE 15. (a) Simulated and measured parameters of the proposed antenna [34]. (b) Expanded view of a prototype of antenna.

TABLE 3. Comparison of dual-band SIW CBSA with different slot configurations.

Ref	Slot geometry	Feeding method	Operating Mode	f_r (GHz)	BW (%)	Pol
[31]	TRS	Microstrip to SIW transition	TE_{110}	9.4, 16	5.9	LP
[32]	Dumbell shaped slot	CPW feed	TE_{120}	9.5, 18	1.5	LP
[33]	Square slot	Inductive window	TM_{310}+ TM_{130} and TM_{320}	21, 26	2.7 2.6	LP
[34]	Two annular exponential slots	GCPW and SIW transition	TM_{010}	37, 48	1.1 1.4	CP

CPW: coplanar waveguide, GCPW: Grounded coplanar waveguide

is formed in the middle layer as a feeding structure. Furthermore, the proximity-coupled slot is inscribed on the bottom layer to improve the impedance matching, and a matching post is utilized. The construction details of the three layers are indicated in Fig.16(a).

Proximity coupled slot aperture couples the energy to a circular cavity single element by exciting the TM_{020} and TM_{120} modes. The 2×2 circular cavity-backed slot array prototype achieved a gain of 13.2dBi at 28GHz and 14.6dBi at 38 GHz for 5G application, as clearly indicated in Fig.16(b). if we look into the geometry of the circular cavity, the radius of the SIW circular cavity is calculated from the following Eq. (9). [13]

$$f_{nm0} = \frac{c}{2\pi\sqrt{\mu_r \varepsilon_r}} \cdot \frac{P_{nm}}{R_{eff}} \tag{9}$$

where f_{nm0} is the resonating frequency of the TM_{nm0} mode, c is the free space light velocity, P_{nm} and is the m^{th} root of the n^{th} order Bessel function. The relation between the radius R_c and R_{eff} is calculated with the following Eq. (10) [11]

$$D_{eff} = 2 * R_c - \frac{d_c^2}{0.95 * s} \tag{10}$$

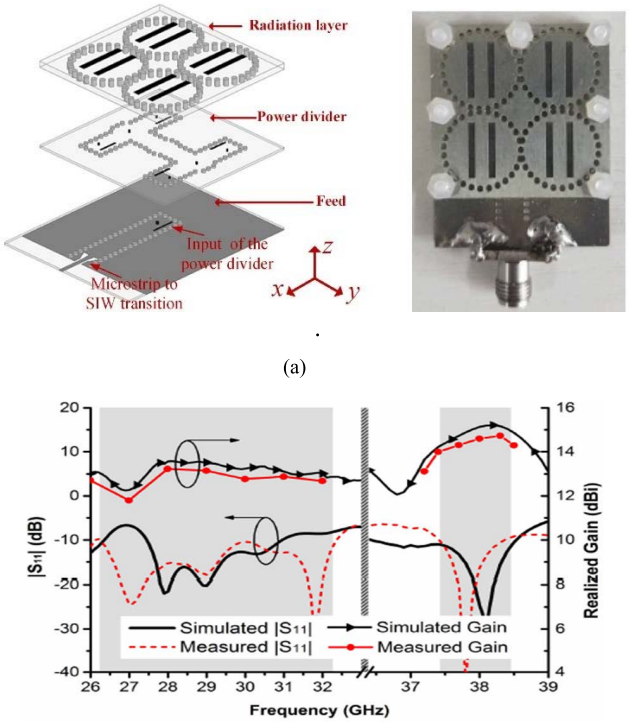

FIGURE 16. (a) a 2×2 SIW circular cavity-backed slot antenna array and fabricated prototype [35]. (b) S parameter and realized gain of the antenna array.

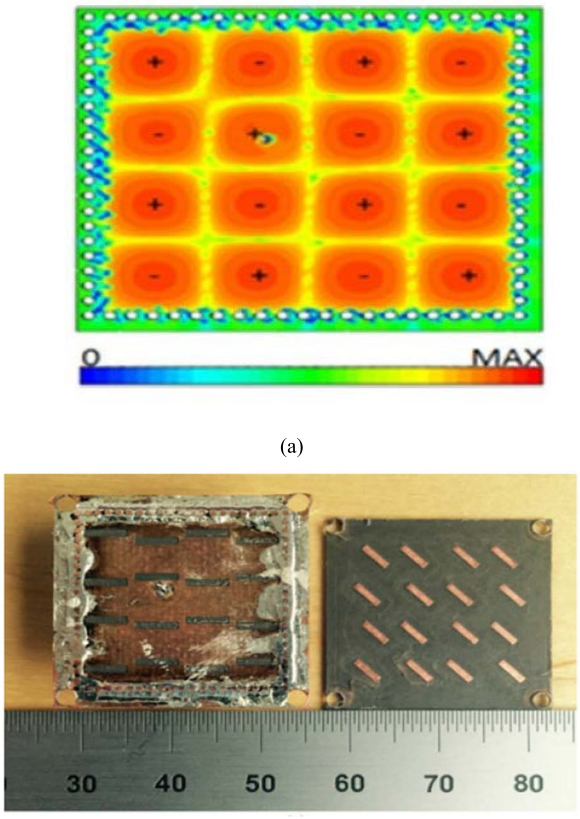

FIGURE 17. (a) TE440 mode field distribution in SIW cavity (b) Prototype of the fabricated antenna with two layers [37].

R_c is the SIW circular cavity radius, D_{eff} is the conventional circular cavity diameter, d_c is the diameter of the metallic vias, and s is the distance between two adjacent metallic vias. $s \leq 2\times d_c$, $d_c/\lambda_\circ < 1$ to ensure that no electromagnetic energy leakage from the cavity as stated above [30], [34], several arrays are implemented through the multilayer substrate, which increases the cost and complexity of the structure, on the other hand, the single layer of substrate SIW cavity slotted array is proposed in [36]. The cavity is loaded with a rhombic slot and a split ring slot resonating on TE_{101} and TE_{102} modes to operate at MMW bands (28 and 38 GHz). The first single element is analyzed later 1 × 4 linear array with a broadband power divider is used to excite four cavity elements. The miniaturized SIW slot antenna array (28.7 × $30.8mm^2$) exhibits impedance bandwidth of 1.05 % and 5.5 % with a realized gain of 10.9 dBi and 12.1 dBi at 28 and 38 GHz, respectively. The measured half-power beamwidth is 20.70^o.

Discussion: In this section, dual-frequency operating antennas are discussed. But these two frequency bands' ratios are small and utilized for specific band applications. Designing a large frequency ratio antenna has wide applications compared to small frequency ratio antennas.

C. CIRCULARLY POLARIZED SIW ANTENNAS

Along with the bandwidth and gain enhancement factors, circular polarization (CP) is an attractive factor for 5G wireless communication. There are several approaches used to achieve CP, for example, dielectric resonator antennas, helical antennas, and crossed dipole utilization, but the complexity and multilayers phenomenon suffer from the issues like nonplanar form and feeding network configuration. A high-gain low-profile CP antenna structure is presented with a multilayer structure [37]. The bottom layer consists of a SIW cavity with 4 × 4 slots inscribed on the top layer of the cavity. The SIW cavity structure is fed with a coaxial cable to excite TE_{440} mode at 28 GHz. The slots in the upper layer of the cavity are arranged on each standing wave peak as shown in Fig. 17 (a) To achieve circular polarization, linear to circular converters are constructed on another substrate layer with dipoles above the slotted cavity as shown in Fig. 17(b). The proposed structure achieves a 16 dBi gain and radiation efficiency of 96% at the Ka-band.

For circularly polarized antennas, AR bandwidth enhancement is a significant factor [38]. A SIW fed antenna exhibit a low AR bandwidth. A simple rotated elliptical cavity fed by slots on the broad sidewall of the SIW is utilized to improve Axial Ratio (AR) bandwidth. By using SIW power dividers, Axial Ratio (AR) bandwidth is improved. A 45^0 rotated elliptical cavity slot is constructed as radiating element fed through a slot on the SIW in the bottom layer.

Earlier, a single elliptical cavity antenna element is analyzed. It exhibits an Axial Ratio (AR) bandwidth of 5.6% and a gain of 7.8 dBi within the operating bandwidth (23-27 GHz). Later 4×4 antenna array with dimensions $50 \times 50 \times 5.3$ mm^3 was designed, simulated Axial Ratio (AR) bandwidth of 21.4 to 29.8 GHz (33%) and operating bandwidth is 22.2 - 27.6 GHz (21.7%) with a peak gain of 18.7 dBi at 27 GHz is achieved. Gain of an antenna can be improved in several methods, i.e., array configuration, utilizing Dielectric Resonator Antenna (DRA), a single circular patch loaded by a conical horn, and Fabry-Perot Cavity antenna, but all these structures are limited to fabrication at MMW bands. In [39], By utilizing the higher-order modes in the cavity an economical wideband, high-gain slotted cavity antenna is constructed for MMW applications. Here a longitudinal slot etched on the top broad wall of the square SIW cavity is fed with a coaxial cable. LP and CP of antennas are analyzed. CP of an antenna is obtained by placing a linear to circular converter above the LP antenna. LP antenna obtains again up to 14 dBi, impedance bandwidth 22.4% by using the proposed structure. Broad bandwidth is achieved by the proximity of exciting modes TE_{310}, TE_{130}, and TE_{330} modes. The proposed CP antenna obtains 11% AR bandwidth and impedance bandwidth in Ka-band.

Discussion: In this section, types of circularly polarized SIW antenna designs are discussed, which are widely used in wireless communications. Practically designing a target-based antenna with this feature is useful for future communications.

D. LARGE FREQUENCY RATIO INTEGRATED ANTENNA

Integration of microwave and MMW antennas has become an important issue in wireless communication. Several designs are reported to operate with a large frequency ratio [40], [41], and [42] but all of them provide a fixed beam direction at MMW bands. But beam steerable with an array of elements is a good choice for mm-wave propagation [4], [43]. A common aperture 5G antenna with dimensions $75 \times 25 \times 0.254$ mm^3 is proposed in [44]. A dipole and tapered slots structures are jointly used to operate at multi bands, i.e., 3.6 GHz and 28 GHz. For the mm-wave tapered slot arrays, the dipole acts as a footprint, and this dipole operates at microwave frequency. Meanwhile, tapered slots are designed to excite a dipole and work as a high-gain antenna at MMW frequency. This design approach achieved a multiband operation and large space coverage of 120° by compact footprint with a realized gain of 8 dBi. The prototype of the large frequency ratio antenna and corresponding results are presented in Fig. 18 (a), (b), and (c).

An aperture-shared antenna with a frequency-switching function is designed for 5G applications [45]. Here a thick patch antenna containing a slotted cavity array (TPCSCA) is presented with two different feeding structures for S-band and Ka-band, as shown in Fig.19(a). For an S-band of operation, TPCSCA operates at TM010 mode. For the Ka-band, TE110 mode is generated through a coaxial probe in the coupling

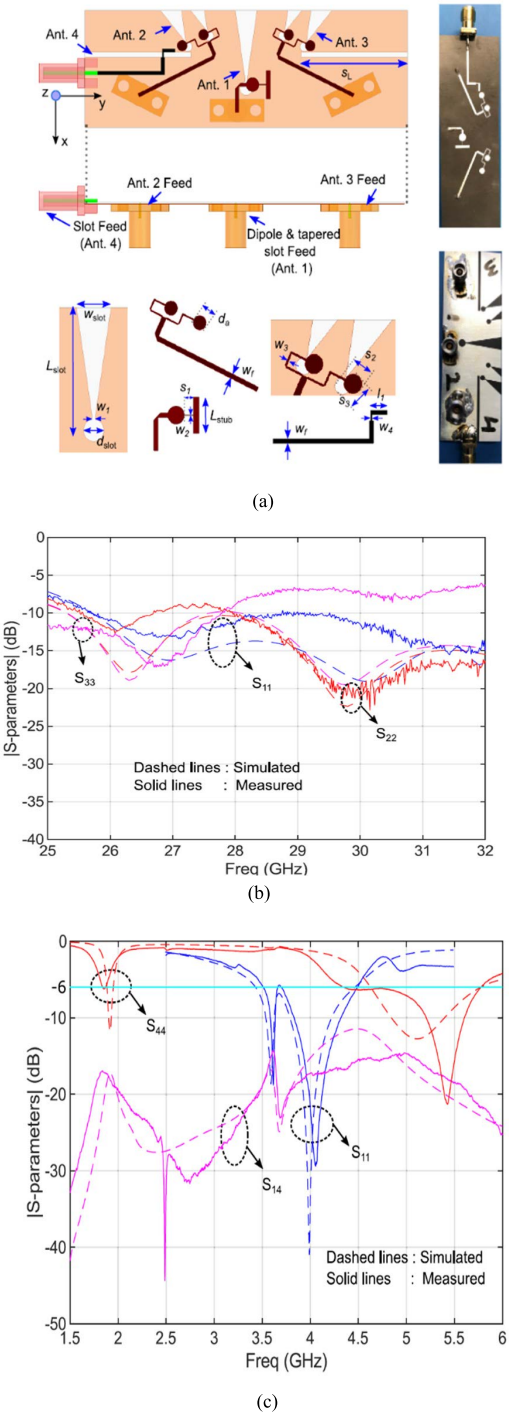

FIGURE 18. Integrated antenna system with dipole and tapered slots (a) simulated view of the antenna and fabricated prototype (b) S parameter results at 28 GHz. (c) S parameter results at sub 6 GHz [44].

layer. This dual-frequency antenna covers ±40° beam steering operation in Ka-band, as shown in Fig.19 (d).In [46], a 28 GHz beam steerable four-element array is integrated into a 3.5 GHz dipole antenna. The SIW technique is used to integrate both antennas and maintain the radiation characteristics without mutual interference. These two antenna elements are fed with two different feeding structures, which facilitate the beam steering conditions at 28 GHz.

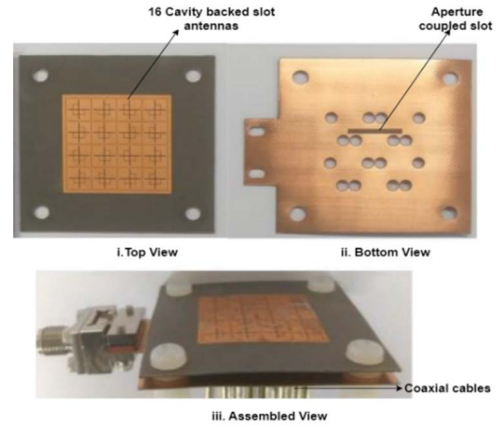

(a)

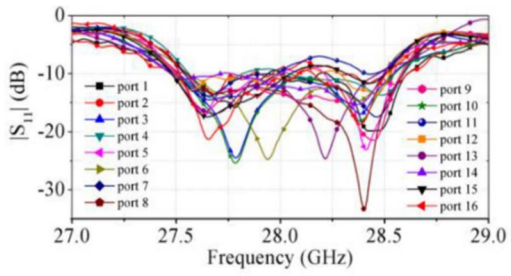

(b)

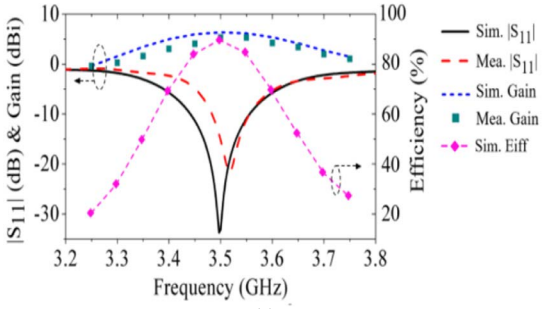

(c)

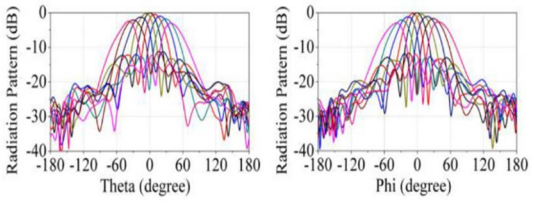

(d)

FIGURE 19. Thick Patch Containing Slotted Cavity Array (TPCSCA) (a) Fabricated prototype antenna details. (b) Measured S- parameter results at Ka-band. (c) simulated and measured Return loss, gain, and efficiency results at the S-band (d) Radiation characteristics of the antenna at the Ka-band [45].

With beam steering and dual-frequency operation capability, the proposed technique is suitable for Satcom terminals applications. Instead of two different ports for large frequency ratio antennas, a single port aperture-fed dual-band antenna

TABLE 4. Large Frequency ratio integrated antennas performance evaluation.

Ref	f_r (GHz)	IBW (%)	Gain (dBi)	Beam Steering	Dual Pol	FR
[44]	1.9,3.5, 5.5 & 28	3.6,25,19.60 & 24.5	7-10	Yes ($\pm 60^o$)	No	14
[45]	3.5,28	3.43,3.29	5.35,14.5	Yes ($\pm 45^o$)	Yes	8
[46]	3.5,28	20.7,20.5	7.07,11.31	Yes	No	8
[48]	3.5,60	2.3,2.6	7.3,24	Yes	No	17

Dual-Pol: Dual Polarization, FR: Frequency Ratio.

is proposed in [47]. As shown in Fig.20(a), an annular ring patch antenna element operates at the microwave band, and an inscribed SIW with a longitudinal slot element operates at the MMW band. A 50 Ω microstrip line is employed underneath the bottom substrate to feed the SIW slot element and annular ring elements. The structure results in misalignment in-field distribution. It can be resolved by placing an annular ring with a small radius to combine the fields. As shown in Fig. 20(b) proposed structure achieves a gain of 10.4 dBi at the C band and 8.51 dBi at the Ka-band, and a good amount of frequency ratio is achieved. The CP is obtained by replacing the annular ring patch antenna element with a circular patch antenna containing shorting vias and stubs, as shown in Fig.20(d). The structure radiates in circular polarization at the microwave band and linear polarization at the MMW band, providing a gain of 4.5 dBi/9.37 dBic as shown in Fig.20(d). A thick patch antenna working at 3.5 GHz and a 12 × 12 SIW slot array antenna operating at 60 GHz is proposed as a dual-band large frequency ratio antenna [48]. The main advantages of this work are high aperture reuse efficiency and high channel isolation between different antennas. This design achieves large Radiating Aperture Reuse (RAR) efficiency of 77%.

Furthermore, by introducing a compact microstrip resonant cell [CMRC] structure of better than 100 dB, isolation is achieved between two antennas at 60 GHz. The frequency ratio of the proposed work is 17, which is utilized for space communication. Comparisons of some of the discussed large frequency ratio integrated antennas are listed in Table 4.

Discussion: In this section, Large frequency ratio antenna designs and characteristics are discussed. These antennas cover microwave and MMW band applications. In future design, an adaptive beam steerable antenna is a good choice for communication.

E. SIW CAVITY-BACKED DUAL SLOT ANTENNAS

For MMW communication, the SIW CBSA array is based on double slots presented in [49]. Here double slot structures are used as radiating elements instead of previously discussed slot structures. The introduction of dual-slot controls the radiation over a wide bandwidth. Single-slot and double-slot radiators are evaluated and compared to know the double-slot performance characteristics. An array of double slots is excited with TE_{320} mode by a corporate feeding network consisting of rectangular coupling apertures fed with coaxial

(a)

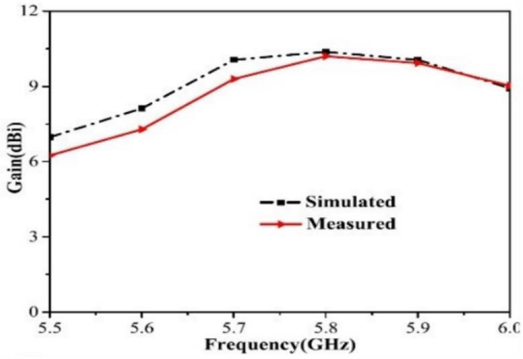

(b)

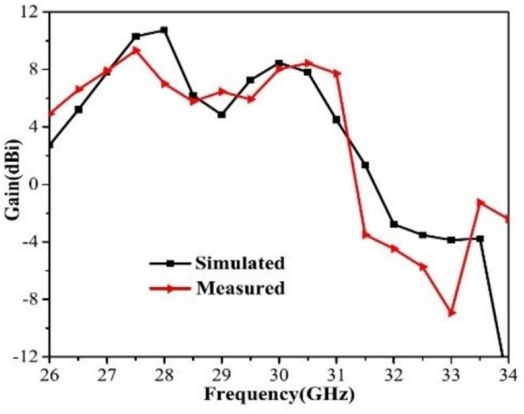

(c)

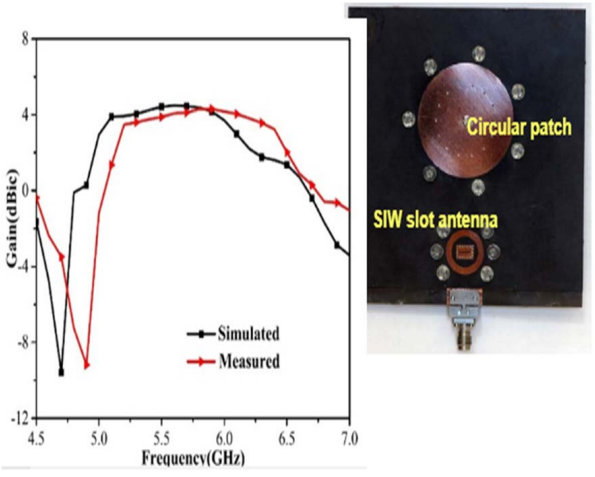

(d)

FIGURE 20. (a) Large frequency ratio single-port antenna (b) Gain characteristics at C band (c) Gain characteristics and Ka-band. (d) CP large frequency ratio single port feed antenna and Gain (dB) characteristics at the C band [47].

cable. The detailed structure and field excitation is presented in Fig.21 (a) and (b). After parametric analysis of the single slot and double slot array in CST studio, it is concluded that the double slot array provides more freedom to choose desired frequency bands. A compact wideband two-port SIW antenna with a central double-slotted metallic plate bounded by two paired corrugations for radar application was proposed in [50] to operate in the X band. Wideband characteristics are achieved by combining transversal slot resonance and higher-order mode resonance of the SIW cavity. After investigating modal analysis without the SMA connector, with the SMA connector of the central slot in the cavity, it concluded that TE_{103} and TE_{302} modes are excited in the SIW antenna with the central slot.

As in [50], double slots are used as radiators to obtain good radiation over a large bandwidth in the X-band and slot resonant length depends on its offset position regarding the SIW centre axis. The second slot is placed across the centre

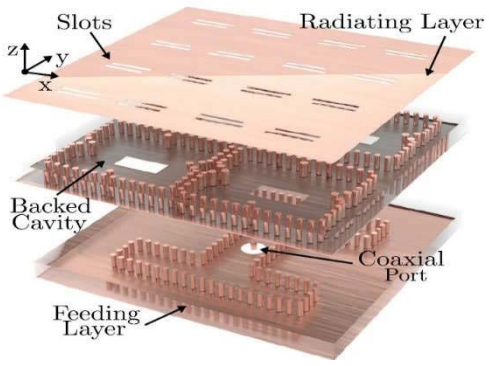

(a)

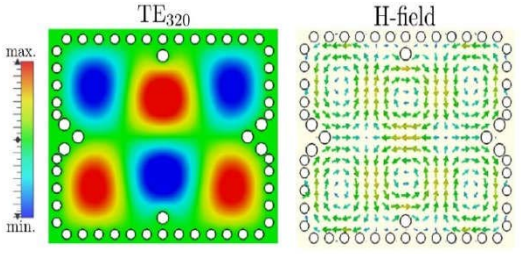

(b)

FIGURE 21. SIW cavity-backed antenna with 4 × 4 double slot array [49]. (b) Electric and magnetic field excitation in SIW cavity through double slot [49].

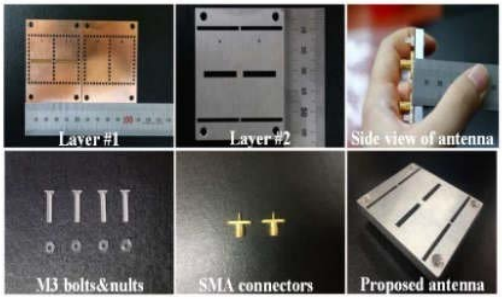

FIGURE 22. SIW antenna with central double-slotted [50].

axis of SIW and acts as a passive element. The second slot, placed slightly away from the axis, acts as an active element. A metallic post placed near the double slot acts as a reflector that enhances radiation. The detailed antenna structure is shown in Fig. 22.

In [51] an H-shaped subarray with four slot pair system is used to improve the impedance matching over a large operating bandwidth as shown in Fig. 23. As discussed, these double slot antennas improve the performance characteristics but they occupy a large area.

A simple technique for the bandwidth enhancement of a CBSA is achieved by placing a via hole above the slot instead of double slots, as shown in Fig. 24 [52]. Here an H -shaped

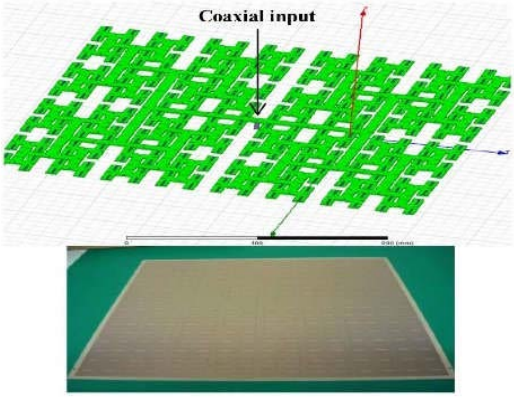

FIGURE 23. Single-layer H-shaped slotted array in SIW technology [51].

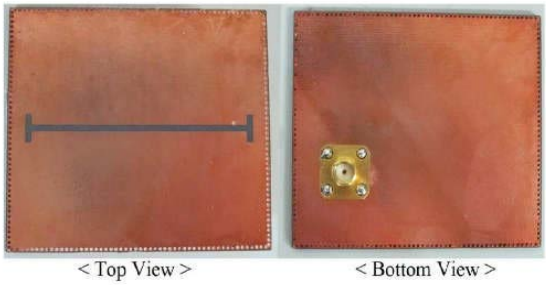

FIGURE 24. SIW H-shaped slot antenna with via hole configuration [52].

slot is used to decrease the resonant slot length, and via hole, position is optimized above the slot for dual resonance first. The slot via hole creates the second resonance without using double slots and enhances the bandwidth in the limited area.

Discussion: In this section, dual slot-based SIW antenna designs are discussed. This new method improves bandwidth performance, and all other radiation characteristics make it suitable for future communications.

F. RECONFIGURABLE SIW ANTENNA

Reconfigurable Radio Frequency Microelectromechanical system (RF-MEMS) antennas were first introduced by E.Brown in 1998 [53]. However, conventional Reconfigurable pattern antennas require expensive solid-state phase shifters and create higher insertion loss at high frequencies. Moreover, the microstrip antennas suffer from losses at a higher frequency. Hence Reconfigurable MEMS switches used in SIW technology for pattern reconfiguration are proposed in [54]. Sekar et al. proposed a new technique to tune the SIW filters by loading the SIW cavity with tunable posts [55]. These posts are controlled by PIN diodes. The field distribution inside the cavity is manipulated. Instead of directly loading the slots with a fixed length, slot length is varied by adding switches to the slot, and the field variation parameter is considered to tune in the SIW CBSA antenna [56]. Four shorting post behaviour depends on the switching mechanism of the PIN diode. Connecting the shortening post

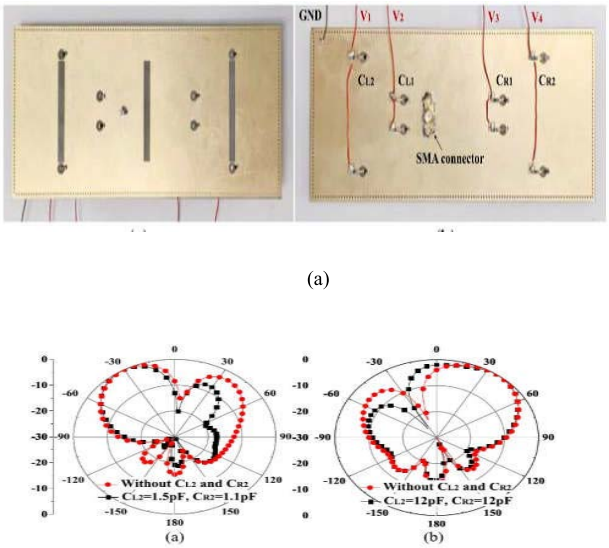

FIGURE 25. Fabricated prototype of SIW CBSA with post-loaded varactor for beam scanning (b) simulated radiation patterns of a fabricated prototype with and without varactors scanning from −30° to 41° [57].

alters the field inside the cavity, and the switching configuration of four posts exhibits different tuning stages that achieve octave band tuning. Via post positions have been chosen by observing the resonance contours inside the SIW CBSA. Here, single via post effect and four via post effects are analyzed for frequency reconfigurability in the octave band (1.1-2.2 GHz). So to achieve wide bandwidth, PIN diodes are used in SIW CBSA. We can reconfigure the antennas in terms of polarization, pattern and frequency for different applications. Here simple beam scanning SIW CBSA using a post-loaded varactor is presented [57], where the pattern reconfigurable has shown a good advantage over phased arrays in terms of size and flexibility to model antenna arrays. The beam steering with reconfiguration is achieved by electronically controlling the state of switches on the SIW aperture [58]. Four wide dipoles are used to generate the beams, and the corresponding aperture is switched on to excite the dipole. In [59], RF-micro electro-mechanical system switches are used in single-arm spiral antennas to reconfigure the radiation pattern. In [60], SIW CBSA with frequency, polarization, and radiation pattern agility was realized. In [57], a SIW CBSA with three transversal radiating slots and placing 16 varactors in a paired form in the vicinity of the longitudinal centerline is proposed to scan the main beam in a different direction, which is presented in Fig.25(a). the junction capacitance of the varactor controls the amplitude and phase of the fields across the slot. As shown in Fig. 25(b), the main beam directions change from −30° to 41° after applying four sets of bias voltages to varactors at 2.6 GHz. Here beam steering can be achieved by employing varactor diodes in SIW CBSA.

In [61], a reconfigurable SIW antenna with H-shaped slots for beam scanning is proposed. Here H shaped slot

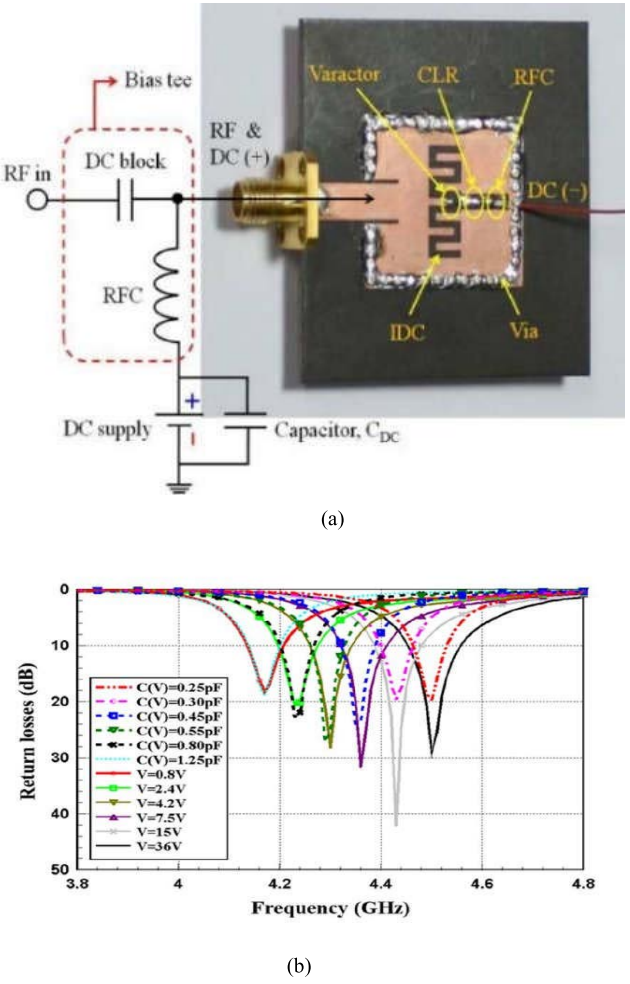

FIGURE 26. (a)Frequency Reconfigurable SIW-IDC slot antenna loaded with varactor diode (b) Simulated and measured return loss of SIW-IDC slot antenna with bias voltage 0V to 36 V. [62].

is designed as a central longitudinal slot that does not cut the surface current, so to radiate the slot, four transversal slots are associated with exciting the currents. These four transversal slots are loaded with PIN diodes. The shape of the slot (L, U, S) depends on the state of PIN diodes (ON/OFF). The radiation characteristics are changed by altering the current flow on the radiation aperture by changing the shape of the slot. The proposed antenna exhibits eight different phase shifts by controlling the length of the shape of the slot and beam scanning between ±45° in the same plane. A novel frequency reconfigurable SIW antenna is proposed in [62] and [63]. In [62], as discussed earlier, miniaturization is achieved by loading the Inter-Digital Capacitor (IDC) slot on SIW, which resonates in Zeroth Order Resonance (ZOR). Apart from miniaturization, frequency tuning is achieved by loading the IDC slot with a varactor diode and proper bias network. The detailed structure is shown in Fig.26 (a). From Fig.26(b), results provided that 9% frequency tuning (4.13 GHz- 4.50 GHz) by changing the bias voltage from 0 V to 36 V.

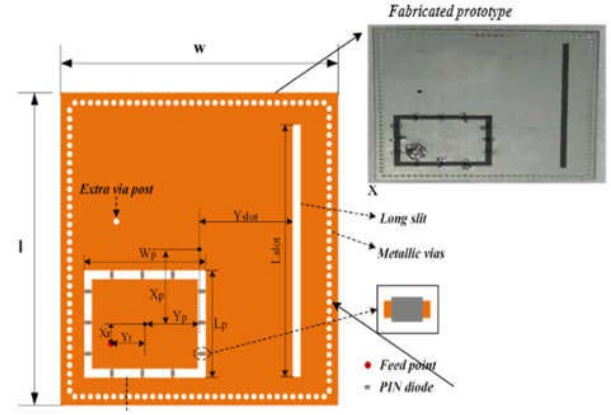

(a)

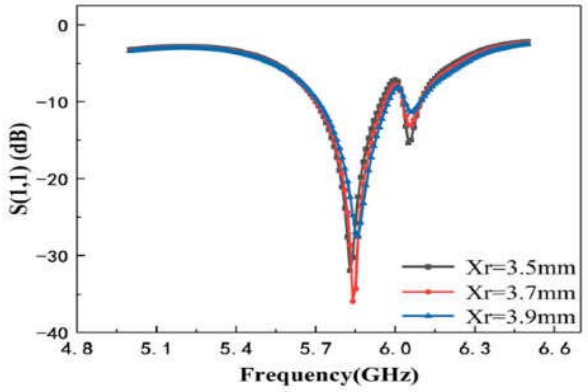

(b)

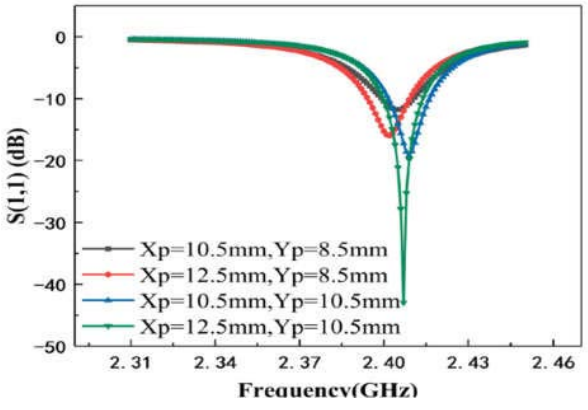

(c)

FIGURE 27. (a)Frequency Reconfigurable Antenna used in S and C band o (b) simulated return loss at C band (c) simulated return loss S-band [63].

SIW frequency reconfigurable antenna switching from S to C band is proposed [63]. A rectangular slot and longitudinal slot are inscribed on the SIW cavity top layer. Twelve PIN diodes (SMP1345) are wired together in a specific order along the rectangular ring slot. The detailed construction is shown in Fig. 27(a). The coaxial bias tee provides biasing to

(a)

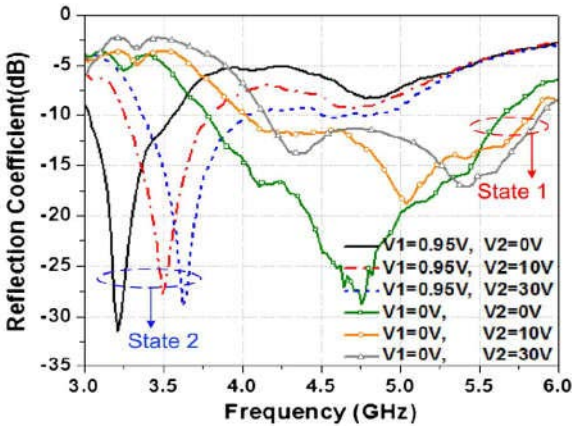

(b)

FIGURE 28. (a) Reconfigurable bow-tie antenna (b) Return loss of antenna for different bias voltages [65].

the diodes, and the size of the SIW cavity and rectangular patch facilitates dual-band frequency. Moreover, via post is inserted to adjust the resonant frequency. Xr is the distance of the coaxial feed position from the centre of the C-band patch antenna. Xp and Yp are the distances between the centre of the S-band patch antenna and to C-band patch antenna. Fig. 27 (b) and (c) indicate the return loss characteristics when the Xr, Xp, and Yp are varied.

Reconfiguration of the antenna can be achieved in several ways, as discussed earlier, and PIN diodes are utilized to reconfigure resonant frequency [64], [65] and [66]. In [65], a Reconfigurable bow-tie antenna is proposed here, and a two-sided bow-tie antenna is fed by parallel strips fed with a microstrip line integrated with pair of PIN diodes and varactors to achieve wideband frequency. The proposed reconfigurable bow-tie antenna is shown in Fig. 28(a). As shown in Fig. 28(b), the impedance bandwidth of 15.3-39.7% is achieved at 3-5 GHz by applying a different combination of bias voltages.

As shown in Fig. 29(a), Polarization reconfigurability is presented by controlling the state of Single Pole Double Throw (SPDT) switches connected to the antenna array [67].

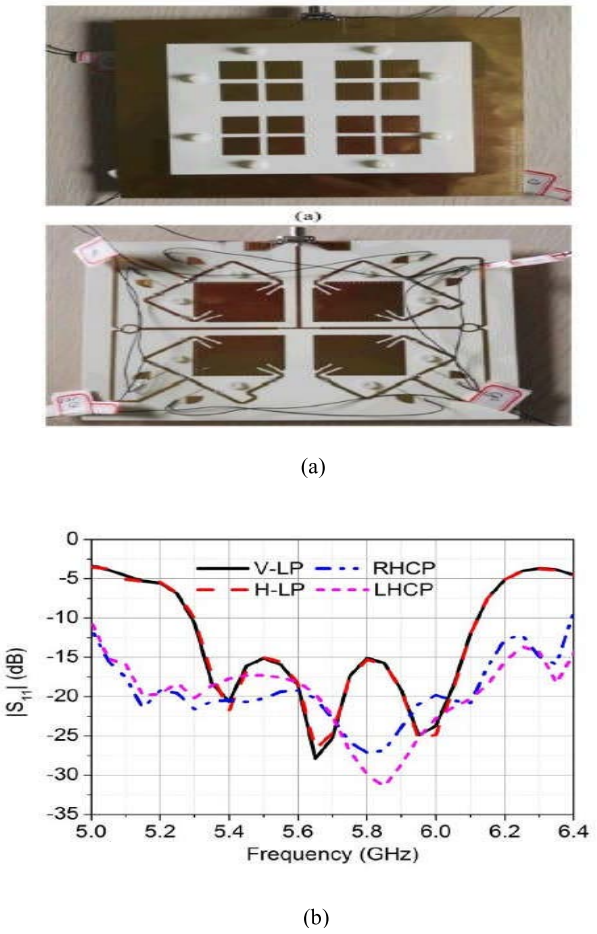

FIGURE 29. Quad polarized reconfigurable SIW antenna (b) Simulated return loss of antenna array for quad polarization states [67].

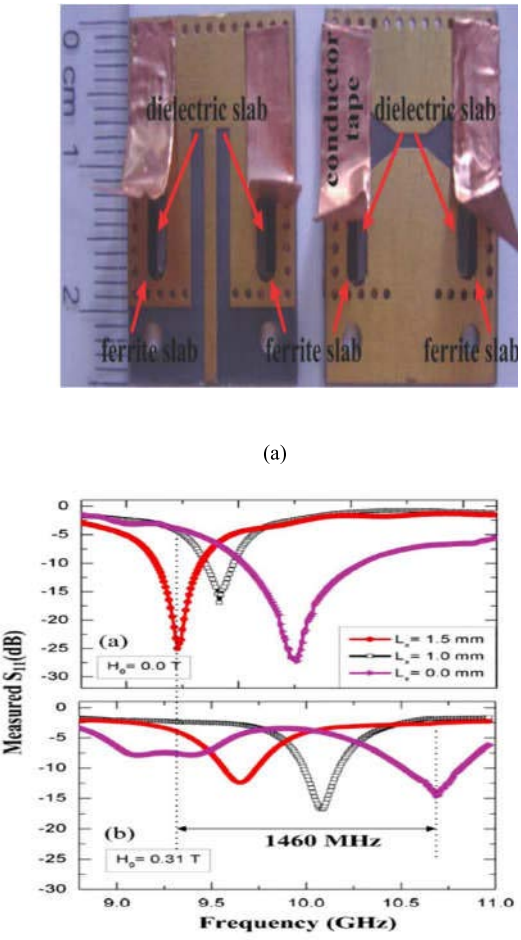

FIGURE 30. (a) Frequency reconfigurable ferrite loaded SIW antenna. (b) Antenna reflection coefficients in bias magnetic fields (H0 = 0 T & 0.31 T) [68].

The antenna array's polarisation can be adjusted between the four polarization modes V-LP, H-LP, LHCP, and RHCP, as shown in Fig. 29(b). These polarization states are achieved by considering a two-layer structure composed of a SIW cavity and four parasitic patches that are excited by ring slots etched onto the surface.

Instead of MEMS and diodes, ferrite slabs are used in the SIW cavity for frequency tuning, as shown in Fig. 30(a) [68]. The position of ferrite slabs alters the field distribution in the cavity, which alters the antenna's resonant frequency. As depicted in Fig. 30(b), the resonant frequency varies as the magnetic field biasing changes.

Discussion: We have discussed frequency, pattern, and polarization reconfigurable antenna designs using switching techniques. These designs may be utilized in multiple applications within a limited area. In the future, these reconfigurable antennas may replace many existing antennas for better performance.

G. TEXTILE SIW ANTENNA

Recent advances in wireless communication make that wearable low-profile textile antennas are presently utilized in various applications, including military, medical monitoring, services, and physical training. All surfaces of the SIW structures, except those with excitation ports, have conducting plates, making them resistant to the impacts of the environment. This characteristic encourages the adoption of SIW antennas in textile antenna design. It is challenging to develop an effective wearable antenna insensitive to the environment. A few textile SIW antenna designs are discussed in this section.

For Wireless Body Area Networks (WBAN), an all-textile SIW cavity-backed circular ring slot antenna was proposed [69]. According to Fig. 31, the suggested antenna is made entirely of textile materials, including felt, conductive fabric, and conductive thread. A semisolid phantom was employed to examine how the human body impacted the results. This one operates at the operating frequency of 5.8 GHz for the ISM band, as shown in Fig. 32. The semisolid phantom effect is negligible, as observed from return loss characteristics. Based on this design, is improving the No.of bands, the operation is a good task for the present scenario. The size of the antenna

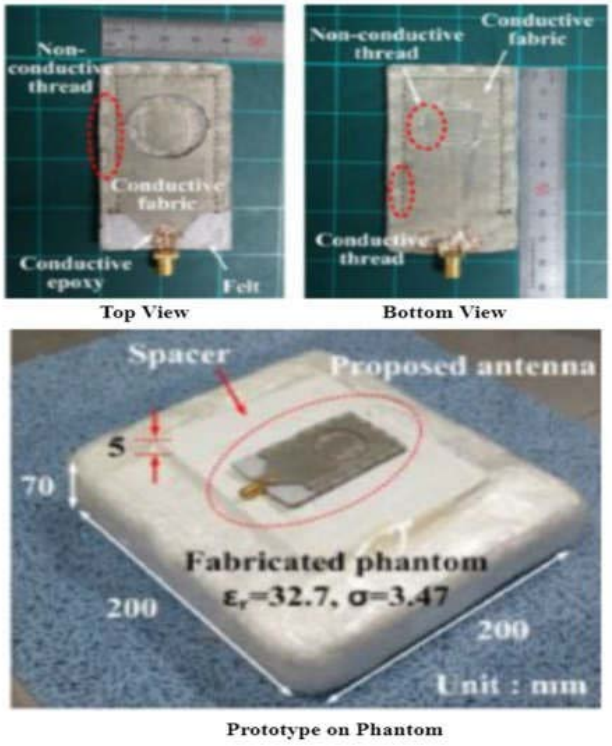

FIGURE 31. Textile SIW cavity-backed circular slot antenna prototype [69].

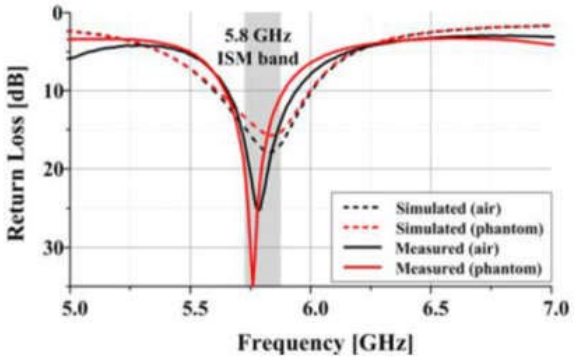

FIGURE 32. Fabricated antenna's returnloss characteristics with and without phantom.

TABLE 5. Critique of SIW technology and GGW technology.

Parameter	SIW	GGW
Design	Easy	Hard
Mass Production	High	Low
Integrability	High	Low
Efficiency	Low	High
Quality factor	Low	High
Bandwidth	High	Low
Substrate	RT5880, Air	Air
Operating bands	Microwave and MMW bands	MMW bands
Machine technology	PCB, LTCC	CNC and Polyjet 3D printer.
Manufacturing cost	Low	High
Dielectric Losses	High	low
Power Handling Capability	Medium	High
Propagating fundamental mode	TE_{10}	TE_{10}
Components	Filters, antennas, power dividers	Filters, power dividers, amplifiers, and antennas

CNC: Computer Numerical Control, Polyjet: Polymer jetting, PCB: Printed Circuit Board, LTCC: Low-Temperature Co-fired Ceramic, GGW: Groove Gap Waveguide.

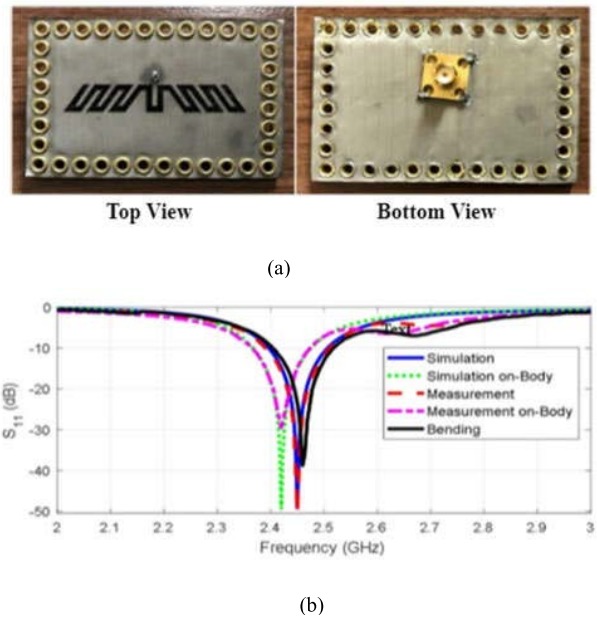

FIGURE 33. (a) Fabricated prototype antenna and (b) Return loss characteristics of the proposed antenna [70].

needs to be reduced. In [70], a SIW textile antenna inspired by metamaterials is proposed for off-body applications to reduce the size. The antenna consists of two layers of wool felt, and conductive fabric Slot configuration exhibits negative order resonance and operates below waveguide cutoff frequency. The prototype is given in Fig. 33. It exhibits a gain of 5.35 dBi, an efficiency of 74.3% and a specific absorption rate (SAR) of 0.38 mw/g averaged over 10g of tissue. It is appropriate for the wearable application at 2.45 GHz. Improving the antenna performance in terms of a band of operation is required.

The Coupled-Mode Substrate Integrated Cavity (CMSIC) antenna with a slotted textile is implemented in [71]. As shown in Fig. 34(a), two coupled cavities comprised of two back-to-back Half Mode Substrate Integrated Cavities (HMSIC), and through the coupling aperture, the probe excites the lower HMSIC and couples it to the upper HMSIC. The antenna prototype with embroidered textile material is presented in Fig. 34(b). This CMSIC antenna offers two resonances, and a slot on the top layer adds a third resonance. The suggested antenna was tested for wearable applications

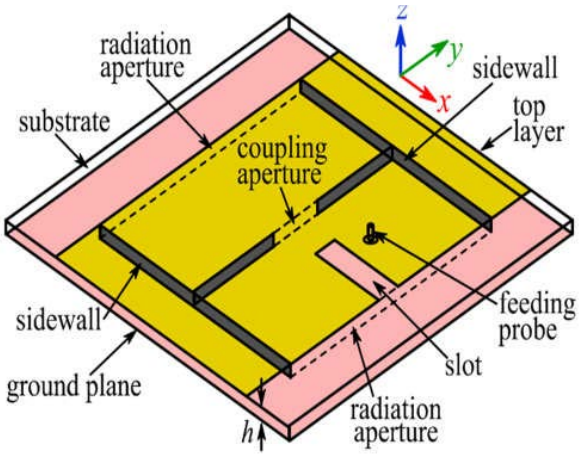

(a)

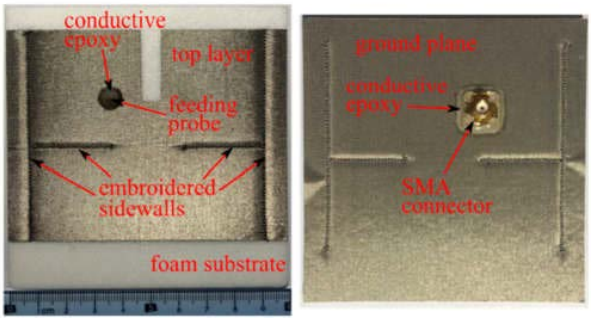

(b)

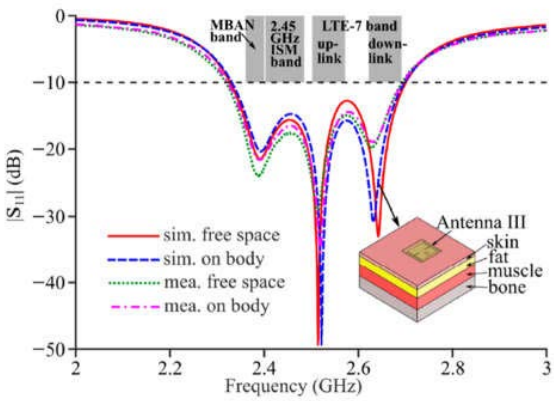

(c)

FIGURE 34. (a) CMSIC antenna structure, (b) prototype antenna with textile material, and (c) Return loss characteristics of the proposed antenna [71].

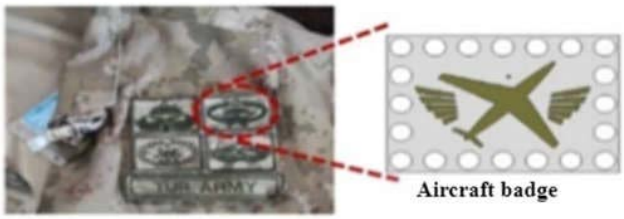

(a)

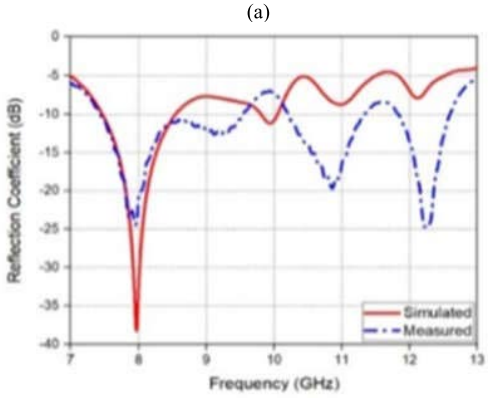

(b)

FIGURE 35. Badge-shaped SIW aircraft-shaped slot antenna. (b) Return loss characteristics of the proposed antenna [72].

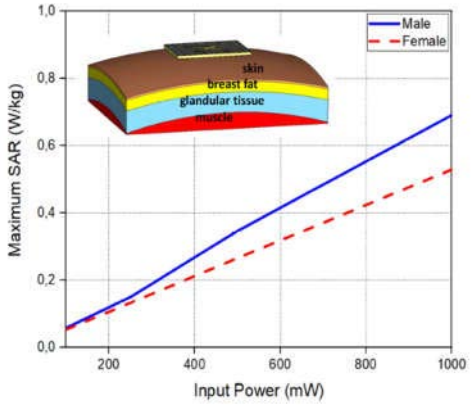

FIGURE 36. Peak SAR variation of the antenna with respect to input power in Males and females [72].

in the Wireless Body Area Network (WBAN), Industrial, Scientific, and Medical (ISM) band, and Long-Term Evolution (LTE) -7 band, as illustrated in Fig. 34(c).

The planar CMSIC antenna used in this work provides a new method for bandwidth expansion on wearable SIW antennas. In one of the HMSICs, the author has recommended a rectangular slot; increasing the number of slots may improve bands of operation. Even slot geometry has a great effect on the bandwidth achieved.

Easily fabricated wearable badge antenna with standard textile material for a military application is presented in [72]. As depicted in Fig. 35(a), a Planar SIW cavity with an aircraft-shaped slot is proposed to be used, which is suited for badge size. Aircraft with meander slots resonating at 8 GHz with 1.05 GHz band. The proposed antenna was tested with on-body performance, and results are provided in Fig. 35(b). Peak Specific Absorption Rate (SAR) value is less than

TABLE 6. Comparison and future scope of different types of SIW cavity-backed slot antennas.

Antenna	Merits	Demerits	Future Scope
Miniaturised Antennas	• Integrability. • Low profile • Economical	• Dielectric losses • Surface waves • Low gain • Low Bandwidth • Single band operation	• High-gain broadband antenna with the multiple-band operation
Dual-band Antennas	• Integrability. • Low profile with dual-band feature. • Feasibility in slot structure.	• Dielectric losses. • Low bandwidth. • Linear polarisation. • Improper frequency ratio.	• High gain broadband, dual-polarised antenna with large frequency ratio
Dual-polarised antennas	• Integrability • Dual-polarization • Broadband • Cross-polarization	• Layers complexity • Substrate loss dominant • Low efficiency	• High-efficient, miniaturized antenna with CP and LP combination
Circularly polarised SIW antennas	• Integrability • CP • Low profile and High Gain • Cross-polarization	• Multilayer structure • Low AR Bandwidth • Shorter-distance communication • Dielectric losses	• Design a single-layer structure with wide AR bandwidth • Beam-steering antenna design is required
Large-Frequency Ratio Integrated antennas	• Integrability • Large frequency ratio operation • Beam steerable condition	• Low gain • Multilayer structure • Beam steering at a fixed angle	• Aperture sharing efficiency improvement • Beam-steering angle optimization
SIW cavity-backed dual-slot antennas	• Integrability • Freedom to choose operating band • High radiation efficiency	• Complex structure • Higher order mode interference • Multilayer structure • Dielectric losses	• Low profile dual slot antenna with beam-steering design is required for next-generation communication
Reconfigurable SIW antennas	• Integrability • Economical • Low profile • Reconfigurability	• Complexity increased by adding switches	• Instead of diodes as switches, any solid-state device implemented with SIW may provide a better result
Textile SIW antennas	• Integrability • Low cost	• Substrate losses • Low efficiency • Low gain	• Design of highly efficient reconfigurable textile SIW antenna with beam scanning used for large-area applications

AR: Axial Ratio, CP: Circular Polarization, LP: Linear Polarization.

30 dBm, as illustrated in Fig. 36, making it appropriate for on-body applications.

Discussion: In this section, low-profile textile SIW antennas are discussed. Present Era, on-body and off-body antennas have been used for ISM applications. Designing a reconfigurable SIW textile antenna with beam-steering capability may be helpful with great importance.

H. A CRITIQUE OF SIW TECHNOLOGY OVER GROOVE GAP WAVEGUIDE TECHNOLOGY

In the MMW band, as the operating frequency increases, transmission losses are increased. Instead of working with transmission lines and coplanar waveguides, a hollow waveguide performs with high efficiency. However, meeting high integration is not an easy task. The gap waveguide model relies upon using boundary conditions to guide electromagnetic wave propagation inside a parallel plate in a specific direction [73]. To understand the analysis between SIW technology [74] and Groove gap waveguide (GGW) technology, summarised data or properties of both technologies is presented in Table.5. After comparison of several parameters, even though GGW technology has several advantages, it is in three-dimensional (3D) structure [75], [76]. GGW components have the capability of high-quality factors making them operate in a narrow band compared to SIW components. Several types of filters, power dividers, amplifiers, and antennas are designed using GGW technology [77].

IV. CONCLUSION

A comprehensive review of Substrate Integrated Waveguide (SIW) cavity-backed slot antenna (CBSA) with different

types of classifications like miniaturized, large frequency ratio, dual-slot, and reconfigurable antennas, textile SIW antennas have been studied in this paper. The antennas reviewed in this paper exhibit different applications like dual-band, dual-polarized, circular polarized, and beam steering, which are essential for 5G communication. Out of all the antenna classifications, the antennas working at a large frequency ratio with a shared aperture are advantageous for wireless applications. Additionally, polarization, frequency, and pattern reconfigurability are achieved easily with reconfigurable SIW CBSA. Achieving this reconfiguration by connecting the diodes to SIW CBSA is advantageous for future applications, and SIW antennas developed with textile materials are discussed for on-body and off-body applications. Finally, designing an aperture-shared SIW CBSA antenna with reconfigurability may be helpful in future communications.

REFERENCES

[1] R. C. Daniels and R. W. Heath, "60 GHz wireless communications: Emerging requirements and design recommendations," *IEEE Veh. Technol. Mag.*, vol. 2, no. 3, pp. 41–50, Sep. 2007.

[2] W. J. Fleming, "New automotive sensors—A review," *IEEE Sensors J.*, vol. 8, no. 11, pp. 1900–1921, Nov. 2008.

[3] S. Oka, H. Togo, N. Kukutsu, and T. Nagatsuma, "Latest trends in millimetre-wave imaging technology," *Prog. Electromagn. Res. Lett.*, vol. 1, pp. 197–204, 2008.

[4] T. S. Rappaport, S. Sun, R. Mayzus, H. Zhao, Y. Azar, K. Wang, G. N. Wong, J. K. Schulz, M. Samimi, and F. Gutierrez, "Millimetre wave mobile communications for 5G cellular: It will work!" *IEEE Access* vol. 1, pp. 335–349, 2013.

[5] D. Loghin, S. Cai, G. Chen, T. T. A. Dinh, F. Fan, Q. Lin, J. Ng, B. C. Ooi, X. Sun, Q.-T. Ta, W. Wang, X. Xiao, Y. Yang, M. Zhang, and Z. Zhang, "The disruptions of 5G on data-driven technologies and applications," *IEEE Trans. Knowl. Data Eng.*, vol. 32, no. 6, pp. 1179–1198, Jun. 2020.

[6] F. Shigeki, "Waveguide line (in Japanese)," Japan Patent 06 053 711, Feb. 25, 1994.

[7] J. Hirokawa and M. Ando, "Single-layer feed waveguide consisting of posts for plane TEM wave excitation in parallel plates," *IEEE Trans. Antennas Propag.*, vol. 46, no. 5, pp. 625–630, May 1998.

[8] H. Uchimura, T. Takenoshita, and M. Fujii, "Development of a 'laminated waveguide,'" *IEEE Trans. Microw. Theory Techn.*, vol. 46, no. 12, pp. 2438–2443, Dec. 1998.

[9] D. Deslandes and K. Wu, "Integrated microstrip and rectangular waveguide in planar form," *IEEE Microw. Wireless Compon. Lett.*, vol. 11, no. 2, pp. 68–70, Feb. 2001.

[10] D. Deslandes and K. Wu, "Integrated transition of coplanar to rectangular waveguides," in *IEEE MTT-S Int. Microw. Symp. Dig.*, vol. 2, May 2001, pp. 619–622.

[11] Y. Cassivi, L. Perregrini, P. Arcioni, M. Bressan, K. Wu, and G. Conciauro, "Dispersion characteristics of substrate integrated rectangular waveguide," *IEEE Microw. Wireless Compon. Lett.*, vol. 12, no. 9, pp. 333–335, Sep. 2002.

[12] F. Xu and K. Wu, "Guided-wave and leakage characteristics of substrate integrated waveguide," *IEEE Trans. Microw. Theory Techn.*, vol. 53, no. 1, pp. 66–73, Jan. 2005.

[13] L. Yan, W. Hong, K. Wu, and T. Cui, "Investigations on the propagation characteristics of the substrate integrated waveguide based on the method of lines," *IEE Proc. Microw. Antennas Propag.*, vol. 152, no. 1, pp. 35–42, Feb. 2005.

[14] M. D. Pozar, *Microwave Engineering*. Hoboken, NJ, USA: Wiley, 2011.

[15] J. Hirokawa, H. Arai, and N. Goto, "Cavity-backed wide slot antenna," *IEE Proc. H-Microw., Antennas Propag.*, vol. 136, no. 1, pp. 29–33, Feb. 1989.

[16] M. Bozzi, A. Georgiadis, and K. Wu, "Review of substrate-integrated waveguide circuits and antennas," *IET Microw., Antennas Propag.*, vol. 5, no. 8, p. 909, 2011.

[17] L. Yan, W. Hong, G. Hua, J. Chen, K. Wu, and T. Jun Cui, "Simulation and experiment on SIW slot array antennas," *IEEE Microw. Wireless Compon. Lett.*, vol. 14, no. 9, pp. 446–448, Sep. 2004.

[18] Y. Dong and T. Itoh, "Miniaturized substrate integrated waveguide slot antennas based on negative order resonance," *IEEE Trans. Antennas Propag.*, vol. 58, no. 12, pp. 3856–3864, Dec. 2010.

[19] A. P. Saghati, A. P. Saghati, and K. Entesari, "An ultra-miniature SIW cavity-backed slot antenna," *IEEE Antennas Wireless Propag. Lett.*, vol. 16, pp. 313–316, 2017.

[20] A. Vallecchi and G. B. Gentili, "Microstrip-fed slot antennas backed by a very thin cavity," *Microw. Opt. Technol. Lett.*, vol. 49, no. 1, pp. 247–250, Jan. 2007.

[21] D. Sievenpiper, H. P. Hsu, and R. M. Riley, "Low-profile cavity-backed crossed-slot antenna with a single-probe feed designed for 2.34-GHz satellite radio applications," *IEEE Trans. Antennas Propag.*, vol. 52, no. 3, pp. 873–879, Mar. 2004.

[22] G. Q. Luo, Z. F. Hu, L. X. Dong, and L. L. Sun, "Planar slot antenna backed by substrate integrated waveguide cavity," *IEEE Antennas Wireless Propag. Lett.*, vol. 7, pp. 236–239, 2008.

[23] G. Q. Luo, Z. F. Hu, W. J. Li, X. H. Zhang, L. L. Sun, and J. F. Zheng, "Bandwidth-enhanced low-profile cavity-backed slot antenna by using hybrid SIW cavity modes," *IEEE Trans. Antennas Propag.*, vol. 60, no. 4, pp. 1698–1704, Apr. 2012.

[24] W. Yang and J. Zhou, "Wideband low-profile substrate integrated waveguide cavity-backed E-shaped patch antenna," *IEEE Antennas Wireless Propag. Lett.*, vol. 12, pp. 143–146, 2013.

[25] M. H. Awida and A. E. Fathy, "Substrate-integrated waveguide Ku-band cavity-backed 2 × 2 microstrip patch array antenna," *IEEE Antennas Wireless Propag. Lett.*, vol. 8, pp. 1054–1056, 2009.

[26] Y. Li and K.-M. Luk, "Low-cost high-gain and broadband substrate—Integrated-waveguide-fed patch antenna array for 60-GHz band," *IEEE Trans. Antennas Propag.*, vol. 62, no. 11, pp. 5531–5538, Nov. 2014.

[27] W. Zhao, X. Li, Z. Qi, and H. Zhu, "Broadband and high-gain dual-polarized antenna array with shared vias feeding network for 5G applications," *IEEE Antennas Wireless Propag. Lett.*, vol. 20, no. 12, pp. 2377–2381, Dec. 2021.

[28] Z. Chen, H. Liu, J. Yu, and X. Chen, "High gain, broadband and dual-polarized substrate integrated waveguide cavity-backed slot antenna array for 60 GHz band," *IEEE Access*, vol. 6, pp. 31012–31022, 2018.

[29] Q. Zhu, K. B. Ng, C. H. Chan, and K.-M. Luk, "Substrate-integrated-waveguide-fed array antenna covering 57–71 GHz band for 5G applications," *IEEE Trans. Antennas Propag.*, vol. 65, no. 12, pp. 6298–6306, Dec. 2017.

[30] Z.-J. Guo, Z.-C. Hao, H.-Y. Yin, D.-M. Sun, and G. Q. Luo, "Planar shared-aperture array antenna with a high isolation for millimeter-wave low earth orbit satellite communication system," *IEEE Trans. Antennas Propag.*, vol. 69, no. 11, pp. 7582–7592, Nov. 2021.

[31] T. Zhang, W. Hong, Y. Zhang, and K. Wu, "Design and analysis of SIW cavity backed dual-band antennas with a dual-mode triangular-ring slot," *IEEE Trans. Antennas Propag.*, vol. 62, no. 10, pp. 5007–5016, Oct. 2014.

[32] S. Mukherjee, A. Biswas, and K. V. Srivastava, "Substrate integrated waveguide cavity-backed dumbbell-shaped slot antenna for dual-frequency applications," *IEEE Antennas Wireless Propag. Lett.*, vol. 14, pp. 1314–1317, 2015.

[33] W. Li, K. D. Xu, X. Tang, Y. Yang, Y. Liu, and Q. H. Liu, "Substrate integrated waveguide cavity-backed slot array antenna using high-order radiation modes for dual-band applications in *K*-band," *IEEE Trans. Antennas Propag.*, vol. 65, no. 9, pp. 4556–4565, Sep. 2017.

[34] Q. Wu, J. Yin, C. Yu, H. Wang, and W. Hong, "Low-profile millimeter-wave SIW cavity-backed dual-band circularly polarized antenna," *IEEE Trans. Antennas Propag.*, vol. 65, no. 12, pp. 7310–7315, Dec. 2017.

[35] T. Hong, Z. Zhao, W. Jiang, S. Xia, Y. Liu, and S. Gong, "Dual-band SIW cavity-backed slot array using TM_{020} and TM_{120} modes for 5G applications," *IEEE Trans. Antennas Propag.*, vol. 67, no. 5, pp. 3490–3495, May 2019.

[36] F.-P. Lai, L.-W. Chang, and Y.-S. Chen, "Miniature dual-band substrate integrated waveguide slotted antenna array for millimeter-wave 5G applications," *Int. J. Antennas Propag.*, vol. 2020, pp. 1–10, Oct. 2020.

[37] M. Asaadi and A. Sebak, "High-gain low-profile circularly polarized slotted SIW cavity antenna for MMW applications," *IEEE Antennas Wireless Propag. Lett.*, vol. 16, pp. 752–755, 2016.

[38] Y. Lang, S.-W. Qu, and J.-X. Chen, "Wideband circularly polarized substrate integrated cavity-backed antenna array," *IEEE Antennas Wireless Propag. Lett.*, vol. 13, pp. 1513–1516, 2014.

[39] W. Han, F. Yang, J. Ouyang, and P. Yang, "Low-cost wideband and high-gain slotted cavity antenna using high-order modes for millimeter-wave application," *IEEE Trans. Antennas Propag.*, vol. 63, no. 11, pp. 4624–4631, Nov. 2015.

[40] L. Zhang, K. Y. See, B. Zhang, and Y. P. Zhang, "Integration of dual-band monopole and microstrip grid array for single-chip tri-band application," *IEEE Trans. Antennas Propag.*, vol. 61, no. 1, pp. 439–443, Jan. 2013.

[41] M. Ikram, N. Nguyen-Trong, and A. M. Abbosh, "Realization of a tapered slot array as both decoupling and radiating structure for 4G/5G wireless devices," *IEEE Access*, vol. 7, pp. 159112–159118, 2019.

[42] D. Wang and C. H. Chan, "Multiband antenna for WiFi and WiGig communications," *IEEE Antennas Wireless Propag. Lett.*, vol. 15, pp. 309–312, 2016.

[43] W. Roh, J.-Y. Seol, J. Park, B. Lee, J. Lee, Y. Kim, J. Cho, K. Cheun, and F. Aryanfar, "Millimeter-wave beamforming as an enabling technology for 5G cellular communications: Theoretical feasibility and prototype results," *IEEE Commun. Mag.*, vol. 52, no. 2, pp. 106–113, Feb. 2014.

[44] M. Ikram, N. Nguyen-Trong, and A. M. Abbosh, "Common-aperture sub-6 GHz and millimeter-wave 5G antenna system," *IEEE Access*, vol. 8, pp. 199415–199423, 2020.

[45] J. H. Bae and Y. J. Yoon, "5G dual (S-/Ka-) band antenna using thick patch containing slotted cavity array," *IEEE Antennas Wireless Propag. Lett.*, vol. 20, no. 6, pp. 1008–1012, Jun. 2021.

[46] J. Lan, Z. Yu, J. Zhou, and W. Hong, "An aperture-sharing array for (3.5, 28) GHz terminals with steerable beam in millimeter-wave band," *IEEE Trans. Antennas Propag.*, vol. 68, no. 5, pp. 4114–4119, May 2020.

[47] B. J. Xiang, S. Y. Zheng, H. Wong, Y. M. Pan, K. X. Wang, and M. H. Xia, "A flexible dual-band antenna with large frequency ratio and different radiation properties over the two bands," *IEEE Trans. Antennas Propag.*, vol. 66, no. 2, pp. 657–667, Feb. 2018.

[48] J. F. Zhang, Y. J. Cheng, Y. R. Ding, and C. X. Bai, "A dual-band shared-aperture antenna with large frequency ratio, high aperture reuse efficiency, and high channel isolation," *IEEE Trans. Antennas Propag.*, vol. 67, no. 2, pp. 853–860, Feb. 2019, doi: 10.1109/TAP.2018.2882697.

[49] B. Hammu-Mohamed, A. Palomares-Caballero, C. Segura-Gomez, F. G. Ruiz, and P. Padilla, "SIW cavity-backed antenna array based on double slots for mmWave communications," *Appl. Sci.*, vol. 11, no. 11, p. 4824, 2021.

[50] Y. Jin, H. Lee, and J. Choi, "A compact, wideband, two-port substrate-integrated waveguide antenna with a central, double-slotted, metallic plate flanked by two paired of corrugations for radar applications," *IEEE Trans. Antennas Propag.*, vol. 66, no. 11, pp. 6376–6381, Nov. 2018.

[51] D. Mencarelli, A. Morini, F. Prudenzano, G. Venanzoni, F. Bigelli, O. Losito, and M. Farina, "Broadband single-layer slotted array antenna in SIW technology," *IEEE Antennas Wireless Propag. Lett.*, vol. 15, pp. 263–265, 2016.

[52] S. Yun, D. Y. Kim, and S. Nam, "Bandwidth enhancement of cavity-backed slot antenna using a via-hole above the slot," *IEEE Antennas Wireless Propag. Lett.*, vol. 11, pp. 1092–1095, 2012.

[53] E. R. Brown, "RF-MEMS switches for reconfigurable integrated circuits," *IEEE Trans. Microw. Theory Techn.*, vol. 46, no. 11, pp. 1868–1880, Nov. 1998.

[54] B. Khalichi, S. Nikmehr, and A. Pourziad, "Reconfigurable SIW antenna based on RF-MEMS switches," *Prog. Electromagn. Res.*, vol. 142, pp. 189–205, 2013.

[55] V. Sekar, M. Armendariz, and K. Entesari, "A 1.2–1.6-GHz substrate-integrated-waveguide RF MEMS tunable filter," *IEEE Trans. Microw. Theory Techn.*, vol. 59, no. 4, pp. 866–876, Apr. 2011.

[56] A. P. Saghati and K. Entesari, "A reconfigurable SIW cavity-backed slot antenna with one octave tuning range," *IEEE Trans. Antennas Propag.*, vol. 61, no. 8, pp. 3937–3945, Aug. 2013.

[57] Y. Ji, L. Ge, J. Wang, Q. Chen, and W. Wu, "Simple beam scanning SIW cavity-backed slot antenna using postloaded varactor," *IEEE Antennas Wireless Propag. Lett.*, vol. 18, no. 12, pp. 2761–2765, Dec. 2019.

[58] L. Ge, M. Li, Y. Li, H. Wong, and K.-M. Luk, "Linearly polarized and circularly polarized wideband dipole antennas with reconfigurable beam direction," *IEEE Trans. Antennas Propag.*, vol. 66, no. 4, pp. 1747–1755, Apr. 2018.

[59] C. Jung, M. Lee, G. P. Li, and F. DeFlaviis, "Reconfigurable scan-beam single-arm spiral antenna integrated with RF-MEMS switches," *IEEE Trans. Antennas Propag.*, vol. 54, no. 2, pp. 455–463, Feb. 2006.

[60] L. Ge, Y. Li, J. Wang, and C.-Y.-D. Sim, "A low-profile reconfigurable cavity-backed slot antenna with frequency, polarization, and radiation pattern agility," *IEEE Trans. Antennas Propag.*, vol. 65, no. 5, pp. 2182–2189, May 2017.

[61] S. Imane, L. Hassan, and H. Mohamed, "Active H-shaped slot reconfigurable SIW antenna for beam-scanning," in *Proc. 2nd Int. Conf. Smart Digit. Environ.*, 2018, pp. 172–176.

[62] S. Somarith, K. Hyunseong, and L. Sungjoon, "Frequency reconfigurable and miniaturized substrate integrated waveguide interdigital capacitor (SIW-IDC) antenna," *IEEE Trans. Antennas Propag.*, vol. 62, no. 3, pp. 1039–1045, Mar. 2014.

[63] J. Qin, X. Fu, M. Sun, Q. Ren, and A. Chen, "Frequency reconfigurable antenna based on substrate integrated waveguide for S-band and C-band applications," *IEEE Access*, vol. 9, pp. 2839–2845, 2021.

[64] I. Serhsouh, M. Himdi, H. Lebbar, and H. Vettikalladi, "Reconfigurable SIW antenna for fixed frequency beam scanning and 5G applications," *IEEE Access*, vol. 8, pp. 60084–60089, 2020.

[65] T. Li, H. Zhai, L. Li, and C. Liang, "Frequency-reconfigurable bow-tie antenna with a wide tuning range," *IEEE Antennas Wireless Propag. Lett.*, vol. 13, pp. 1549–1552, 2014.

[66] X. Yang, Y. Chen, L. Ye, M. Wang, M. Yu, and Q. H. Liu, "Frequency reconfigurable circular patch antenna using PIN diodes," in *Proc. IEEE Int. Conf. Microw. Millim. Wave Technol. (ICMMT)*, Jun. 2016, pp. 606–608.

[67] J. Hu, Z.-C. Hao, and W. Hong, "Design of a wideband quad-polarization reconfigurable patch antenna array using a stacked structure," *IEEE Trans. Antennas Propag.*, vol. 65, no. 6, pp. 3014–3023, Jun. 2017.

[68] L.-R. Tan, R.-X. Wu, C.-Y. Wang, and Y. Poo, "Ferrite-loaded SIW bowtie slot antenna with broadband frequency tunability," *IEEE Antennas Wireless Propag. Lett.*, vol. 13, pp. 325–328, 2014.

[69] Y. Hong, J. Tak, and J. Choi, "An all-textile SIW cavity-backed circular ring-slot antenna for WBAN applications," *IEEE Antennas Wireless Propag. Lett.*, vol. 15, pp. 1995–1999, 2016.

[70] M. E. Lajevardi and M. Kamyab, "Ultraminiaturized metamaterial-inspired SIW textile antenna for off-body applications," *IEEE Antennas Wireless Propag. Lett.*, vol. 16, pp. 3155–3158, 2017.

[71] J. Cui, F.-X. Liu, X. Shen, L. Zhao, and H. Yin, "Textile bandwidth-enhanced coupled-mode substrate-integrated cavity antenna with slot," *Electronics*, vol. 11, no. 15, p. 2454, Aug. 2022.

[72] E. Celenk and N. T. Tokan, "All-textile on-body antenna for military applications," *IEEE Antennas Wireless Propag. Lett.*, vol. 21, no. 5, pp. 1065–1069, May 2022.

[73] E. Rajo-Iglesias, M. Ferrando-Rocher, and A. U. Zaman, "Gap waveguide technology for millimetre-wave antenna systems," *IEEE Commun. Mag.*, vol. 56, no. 7, pp. 14–20, Jul. 2018.

[74] F. Xu, Y. Zhang, W. Hong, K. Wu, and T. J. Cui, "Finite-difference frequency-domain algorithm for modeling guided-wave properties of substrate integrated waveguide," *IEEE Trans. Microw. Theory Techn.*, vol. 51, no. 11, pp. 2221–2227, Nov. 2003.

[75] A. Tamayo-Dominguez, J.-M. Fernandez-Gonzalez, and M. Sierra-Perez, "Groove gap waveguide in 3-D printed technology for low loss, weight, and cost distribution networks," *IEEE Trans. Microw. Theory Techn.*, vol. 65, no. 11, pp. 4138–4147, Nov. 2017.

[76] M. Ferrando-Rocher, A. Valero-Nogueira, J. I. Herranz-Herruzo, and J. Teniente, "60 GHz single-layer slot-array antenna fed by groove gap waveguide," *IEEE Antennas Wireless Propag. Lett.*, vol. 18, no. 5, pp. 846–850, May 2019.

[77] B. Ahmadi and A. Banai, "Substrateless amplifier module realized by ridge gap waveguide technology for millimeter-wave applications," *IEEE Trans. Microw. Theory Techn.*, vol. 64, no. 11, pp. 3623–3630, Nov. 2016.

ELAGANDULA APARNA (Graduate Student Member, IEEE) received the B.Tech. degree in electronics and communication engineering from the Jawaharlal Nehru Technological University Hyderabad College of Engineering Jagtial, and the M.E. (M.R.E.) degree from the University College of Engineering, Osmania University, Hyderabad, in 2015. She is currently a full-time Research Scholar with the Department of ECE, National Institute of Technology Warangal, India, with an Institute Fellowship from the Department of Ministry of Human Resource (MHRD). Her research interests include antenna designs for 5G and beyond applications.

GOPI RAM (Senior Member, IEEE) received the B.E. degree in electronics and telecommunication engineering from the Government Engineering College Jagdalpur, Jagdalpur, Chhattisgarh, India, in 2007, and the M.Tech. degree in telecommunication engineering from the National Institute of Technology Durgapur, Durgapur, West Bengal, India, in 2011. In 2012, he joined as a full-time Institute Research Scholar with the National Institute of Technology Durgapur, to carry out research for his Ph.D. degree. He received the Scholarship from the Ministry of Human Resource and Development (MHRD), Government of India, from 2009 to 2011 (M.Tech. degree) and from 2012 to 2016 (Ph.D. degree). He joined NIT Warangal in April 2018, as an Assistant Professor with the Department of ECE, where he is currently working as an Assistant Professor with the Department of ECE. He has published more than 90 research papers in international journals and conferences. His research interests include analysis and synthesis of antenna arrays via bio-inspired evolutionary algorithms, and antenna array optimization of various radiation characteristics.

G. ARUN KUMAR (Senior Member, IEEE) was born in Hyderabad, India, in 1982. He received the B.E. degree in electronics and communications engineering from Osmania University, in 2004, and the M.E.Tel.E. and Ph.D. degrees in electronics and telecommunications engineering from Jadavpur University, in 2006 and 2012, respectively. He joined the Circuits and Systems Division, Society for Applied Microwave Electronic Engineering and Research (SAMEER), Kolkata, India, under the Ministry of Electronics and Information Technology (MeitY), Government of India, in 2010, where he worked as a Scientist B, from 2010 to 2014, and a Scientist-C, from 2014 to 2018. In June 2018, he joined the Department of Electronics and Communication Engineering, National Institute of Technology Warangal, where he is currently an Assistant Professor. He has successfully completed two projects sponsored by DRDO and more than ten projects sponsored by MeitY. His research interests include simulation, modeling, and design of millimeter wave active and passive circuits, MMIC design, metamaterials, time-modulated components, and substrate-integrated waveguide circuits. He is a Life Member of IETE and the Society of EMC Engineers, India. He received the Early Career Research Award from DST-SERB, in 2019.